Fermi National Accelerator Lab

Optical Imaging of the Tevatron Beam using Synchrotron Radiation

a.k.a. Synclite

Randy Thurman-Keup

AD / Instrumentation Deptartment

January 29, 2008

BEAMS-DOC-1975-V2[1]

Abstract

The synchrotron light imaging system, **Synclite**™, was originally installed by Alan Hahn in the early 1990's. It has undergone at least one major hardware upgrade and several DAQ upgrades. The imaging system is a simple one lens telescope. It has various mirrors for redirecting the light, a wavelength filter for isolating the desired source, and an intensified CID camera for capturing the image. The data acquisition and control system is LabVIEW running on a Windows XP PC. This document describes the Synclite system as it presently exists and documents the various studies performed in support of understanding the system.

[1] **BEAMS-DOC-2537** contains a list of all current documentation regarding the Synclite system.

1 Introduction

When a charged particle is bent in an arc, it emits electromagnetic radiation. Under certain circumstances[2], part of this light is in the visible spectrum and can be detected with generic optical devices. Since each particle emits this light, one can point a telescope at it and produce a transverse image of the beam. The Synclite system does this and thus offers a non-destructive method for measuring the transverse emittances of the Tevatron beam when it is at 980 GeV.

1.1 History

The original version of the Synclite system was installed sometime in the early 1990's by Alan Hahn. The original system consisted of tubes to route the light instead of light boxes. Around 1993-1994, the modern version was installed. This was all way before my time, so I don't know what the state of the system was up until Run II started, but at that time confusion set in with regards to the antiproton system. With the optics seemingly in focus, the scale was wrong by 40% when compared to closed-orbit bump data. There were speculations that the spot being focused was really a reflection from an edge further upstream which certainly seemed possible since other reflections could be seen as the pickoff mirror was moved around. There were further attempts to study the problem (including an attempt with an Air Force optical target [9]) but nothing conclusive was discovered. Meanwhile, Alex Valishev pointed out that since the energy went from 900 → 980 GeV in Run II, this would increase the light from the body quite significantly due to the fact that we are observing the tail of an exponential spectrum[3] where the center has shifted by a factor of 2 or 3. This change would be more than enough to make the body light easily visible, and in fact the antiproton spot could be body light and not edge light. This was indeed the problem and recently the mirror was moved in further as a regular part of each store. This allowed it to see the edge light with a corresponding improvement in resolution and scale.

2 Theory

A charged particle that undergoes acceleration in a direction transverse to its motion emits radiation in a cone around its velocity vector. This radiation is called synchrotron radiation after its first observation in a synchrotron (see [1] - [4], [10], [11], and [12] for various theoretical treatments of synchrotron radiation). Today there are many specialized synchrotron light labs around the world, some of which have produced numerical codes for solving synchrotron radiation problems. Synchrotron Radiation Workshop (SRW) [13], developed at ESRF in France, was used for the calculations in this paper. SRW runs within the context of a parent application called Igor Pro [14].

To run SRW, one must input various parameters such as the lattice parameters of the beam, magnetic field configuration, and the physical positions and characteristics of the various optical elements. The one catch is that since this program was written at an electron accelerator, certain parameters are hard coded and cannot be changed. For instance, the particles it assumes for the beam are electrons and there is no way to change that. Hence one must scale the magnetic fields

[2] For the Synclite setup at the Tevatron, these requirements are that the energy of the beam must be > 600-700 GeV and the light must have been emitted near the edge of a dipole magnet. Although at 980 GeV, the light emitted in the body of the magnet is also clearly visible.

[3] If one shifts the center of an exponential-type function by 3 times the decay constant, the change in the height of the tails is not ~3, but is $e^{-(x-a\lambda)/\lambda} / e^{-x/\lambda} = e^{a}$, or 20 for a = 3.

and the beam energy by m_e/m_p. And one must remember to convert a 95% normalized emittance to a RMS non-normalized emittance[4] (which apparently at electron accelerators is expressed in units of nm). If you do try to run this, be warned that it takes a lot of memory (anywhere from 100s of MB to 1 GB), and aliasing is a constant fear. Care must be taken that adjacent grid points don't differ in phase by more than a half wavelength. And in fact, the documentation states that proper sampling size is needed in both coordinate and angular space. Another quirk is the treatment of the finite transverse distribution of the beam. Since it is far too resource consuming to calculate a grid of points representing the Gaussian beam, the shape of the beam is modeled by convolving the illumination from a zero-size beam with a Gaussian representing the beam whose moments are propagated through the optical elements. A consequence of this is that apertures do not affect the imaged beam shape. They only affect shapes resulting from the mixing of edge and body light. Another way to say this is that only light from the central orbit is directly calculated and propagated.

Synchrotron light is emitted when the particles traverse magnets. Since the beam is constantly bending through the magnet, the light sweeps out a path like a lighthouse (Figure 1). In the body of a TeV dipole, the emitted wavelengths peak well into the infrared (~ few μm). Near the edge of a magnet, the emitted wavelengths shift to smaller values just into the ultraviolet (few hundred nm). At micron wavelengths, diffractive effects make it impossible to image a 500μm beam. However, at 400nm, diffractive effects are only 100-200μm allowing a measurement of the beam width. A further advantage in using the shorter wavelength light from the edge of the magnet is that the longitudinal extent of the source of the light is much smaller. Figure 1 shows the illumination at the pickoff mirrors of the Synclite system. The antiproton illumination is smaller since the mirror is closer. These images are calculated at wavelengths of 440 nm for protons and 400nm for pbars. One sees several features in these plots, starting with the bright spot which originates from the magnet edges. In the proton case, this spot originates from a single magnet edge (see Section 3 for details of the physical layout). The body light from this single magnet results in a tail on only one side of the peak (in the horizontal plane). In the antiproton case, there are two edges and thus there are tails on both sides of the peak resulting from the bodies of both magnets. The tail in the proton case is larger because the peak has contributions from only one edge and the wavelength is larger (recall that light from the body peaks at longer wavelengths).

Figures 3 and 4 show the expected number of photons as a function of wavelength for protons and antiprotons. They also show the illumination at the pickoff mirror for various wavelengths between 200 nm and 1000 nm. The strange 200 nm distribution for the antiprotons is interference between the two magnet edges and is demonstrated further in Figure 5. For a typical proton bunch size of 250 x 10^9, we expect ~6 x 10^5 photons / bunch / 25nm bandwidth. For the more and more typical pbar bunch sizes of 100 x 10^9, we expect ~7.5 x 10^5 photons / bunch / 25nm bandwidth.

[4] The emittance in SRW is related to the typical Tevatron 95% normalized emittance by $\varepsilon_{SRW} = \varepsilon_{95\%} / 6\pi\gamma$.

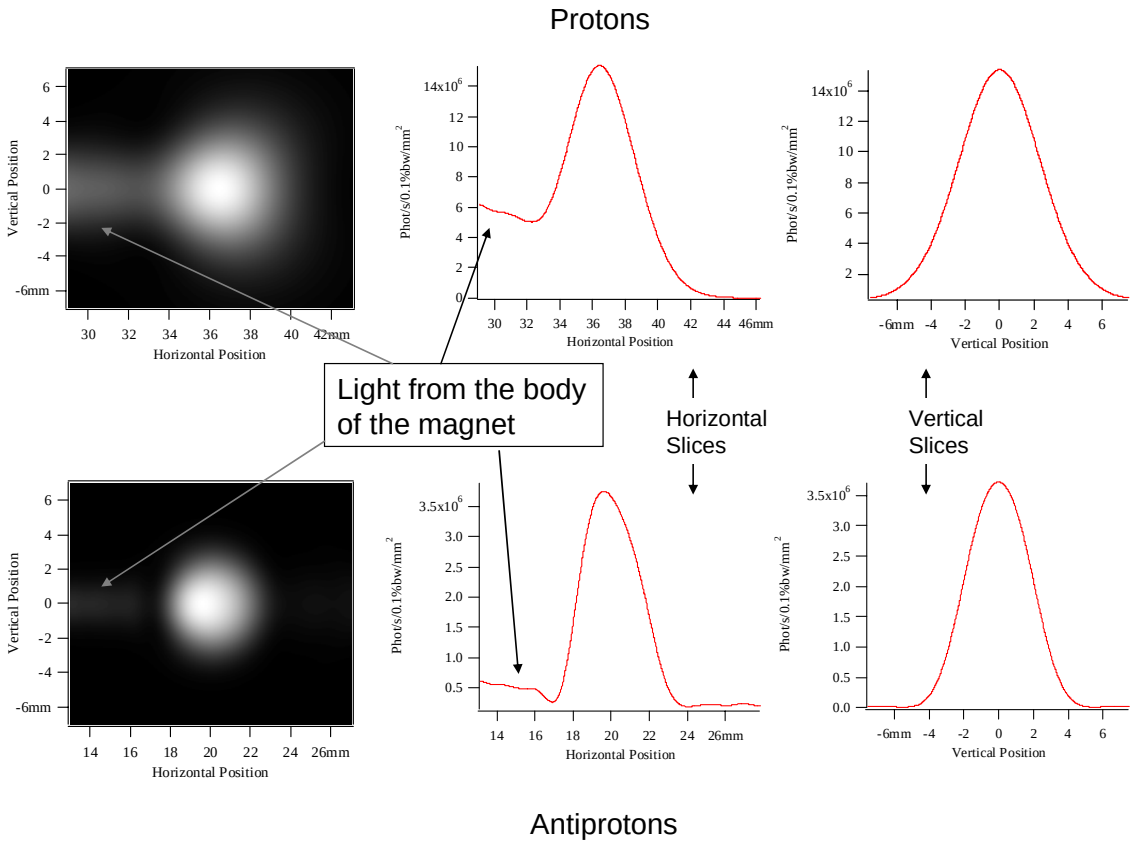

Figure 1: Synchrotron light images for proton (top) and antiproton (bottom) beams.

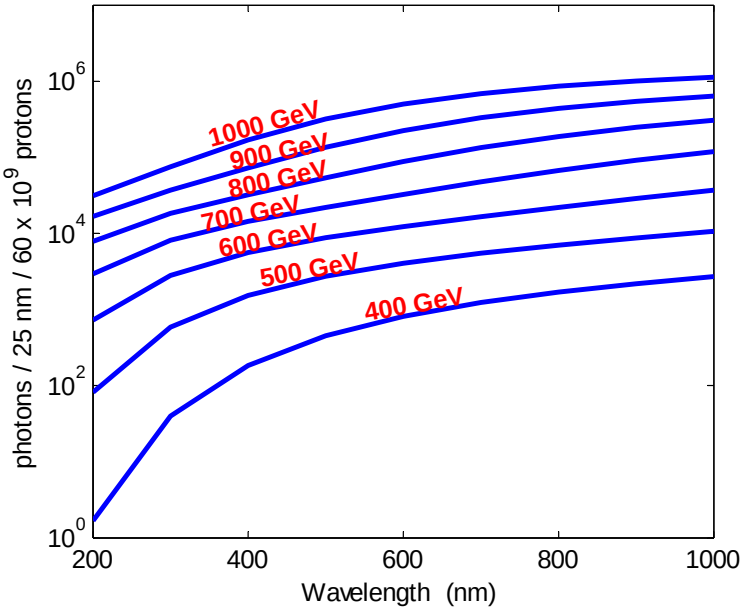

Figure 2: Optical intensity as a function of wavelength at several beam energies.

Protons

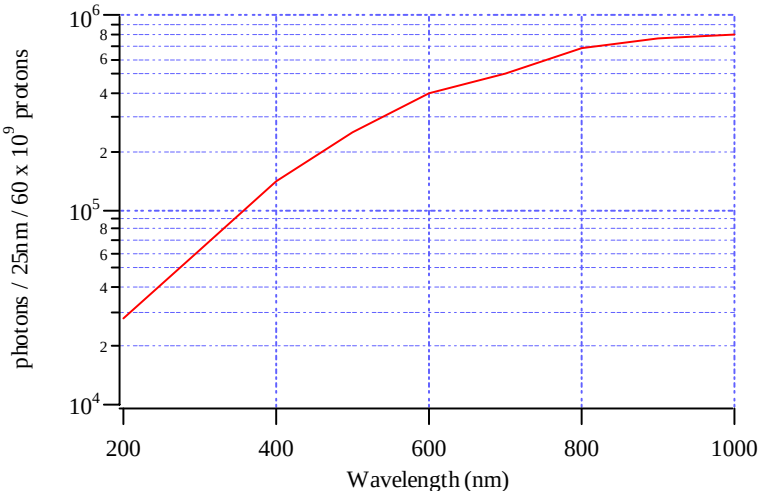

Illumination at pickoff mirror

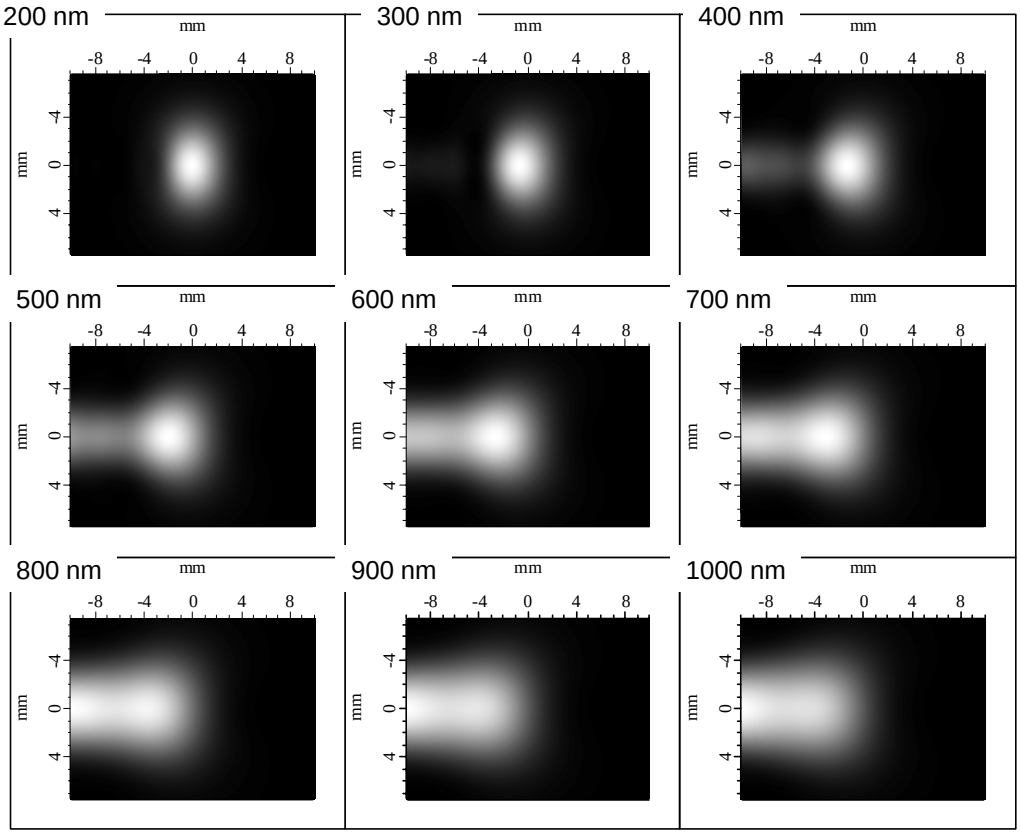

Figure 3: Integrated light intensity vs. wavelength (top), and illumination sequence as function of wavelength (bottom).

Antiprotons

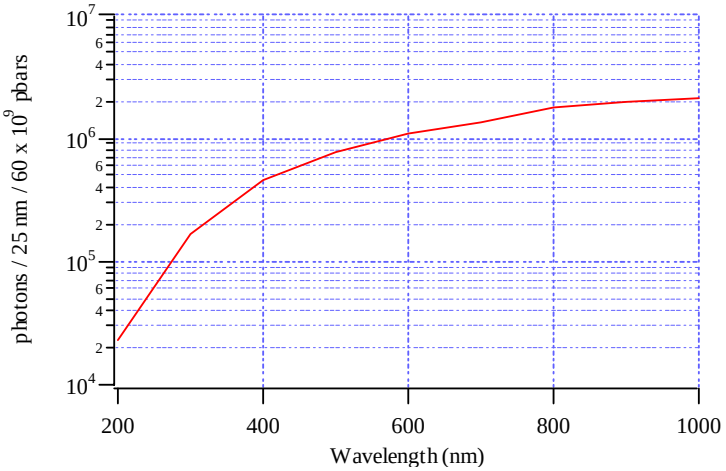

Illumination at pickoff mirror

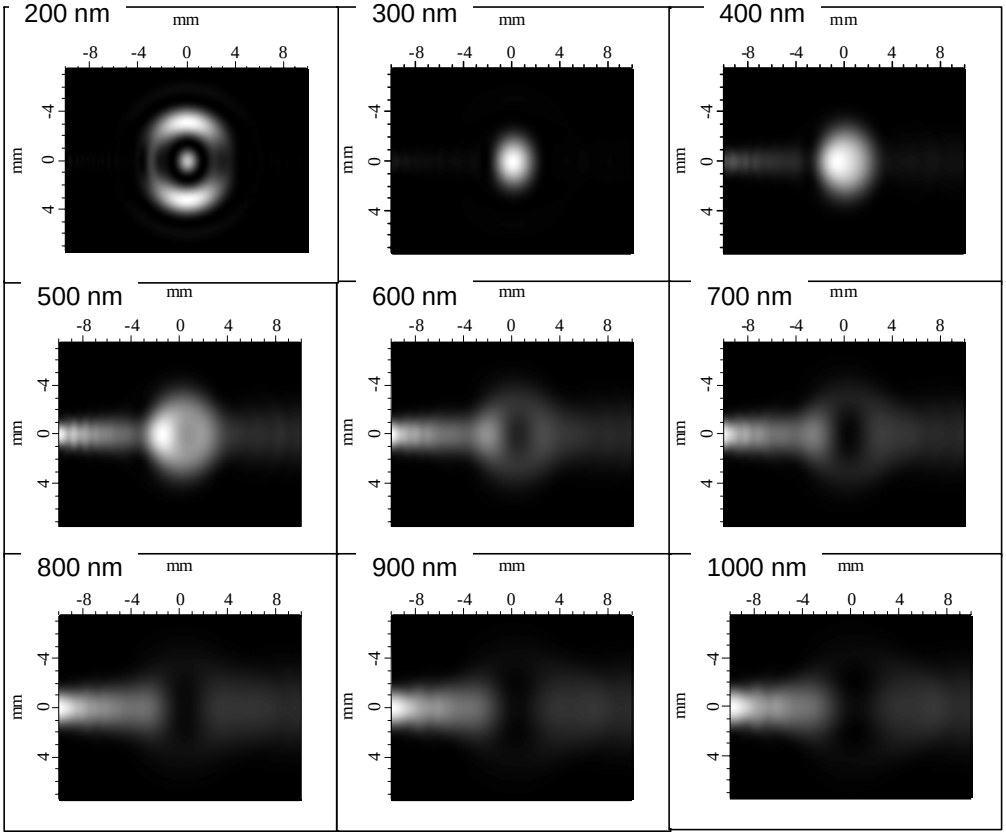

Figure 4: Integrated light intensity vs. wavelength (top), and illumination sequence as function of wavelength (bottom) for antiprotons.

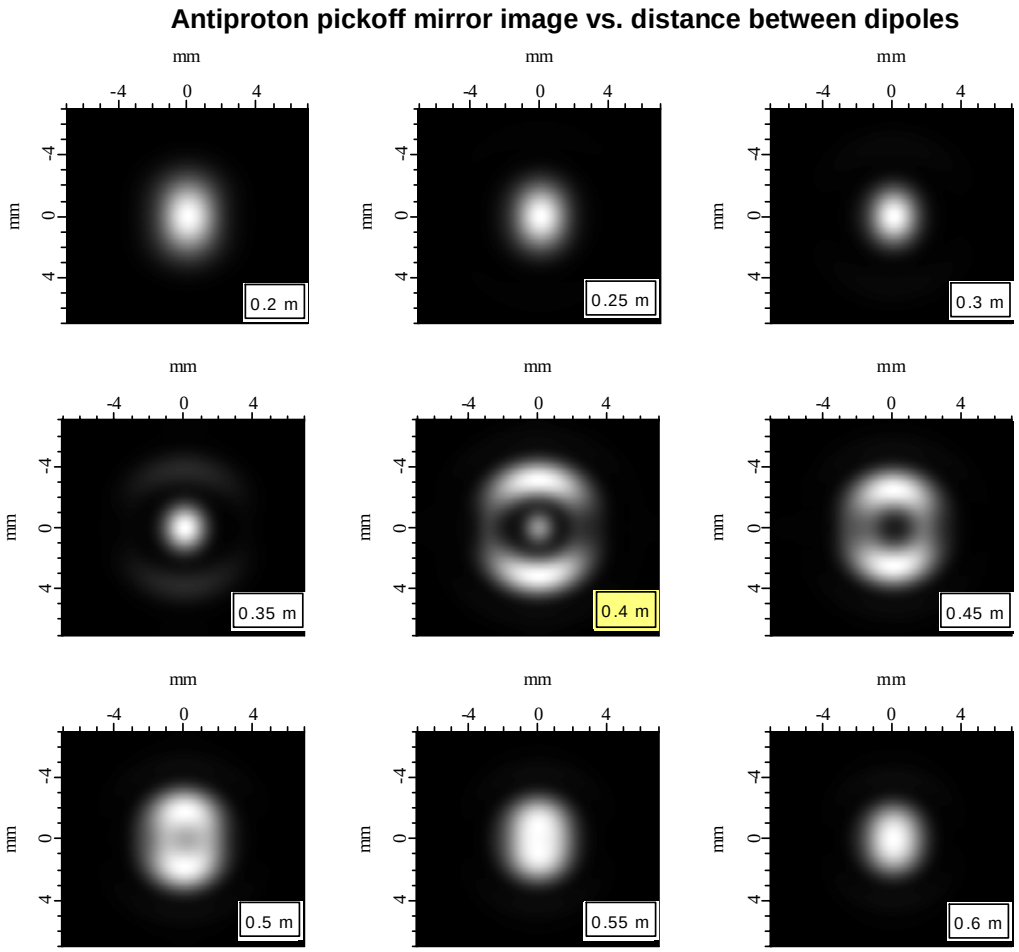

Figure 5: Variation in antiproton images as a function of the distance between the two contributing edges of the dipoles as seen at a wavelength of 200 nm. The nominal distance is 0.4m (highlighted in yellow). The interference arises because photons emitted at the first edge are approximately ½ of a wavelength ahead of the proton when they reach the second dipole edge and the process of entering a magnet produces a wave that is 180° out of phase with that produced by exiting a magnet.

3 Apparatus

The Synclite devices (proton and antiproton) are located in the Tevatron at C11 and are each comprised of a 1.5" square moveable mirror inside the beampipe which intercepts and redirects the synchrotron light out the side of the beampipe through a quartz vacuum window [17] to a light tight box. The box is connected to the beampipe proper through a rubber boot. Inside the box, the light traverses a lens [18] and hits a moveable X-Y mirror. In the proton box, the light then may encounter an optional neutral density filter with a transmission of 4.2%, and a beam splitter [19] which sends half the light to the Abort Gap Monitor (AGI) [20]. The neutral density filter is mounted on a moveable support which can be inserted and retracted. Next the proton light hits another moveable X-Y mirror before passing through the filter wheel [19]. In the antiproton box, after reflection from the initial X-Y mirror, the light traverses a blue filter [19]. In both boxes, the post-wavelength filter light is received by the combination Image Intensifier [21] and CID camera [22]. The output of the CID camera is processed by the controller which sends an RS-170 video signal out of the tunnel to a framegrabber card which is read by a Windows XP PC running LabVIEW [15]. Figures 6 through 10 show the layout of the apparatus

from various perspectives. Mechanical drawings of the beampipe pieces can be found on the drafting web site under the AD mechanical support web page, typically with titles that include the phrase “Synchrotron Light Monitor Mark II”.

Note: Drawings showing details of the Synclite boxes are not accurate, however the beampipe related stuff seems to be correct.

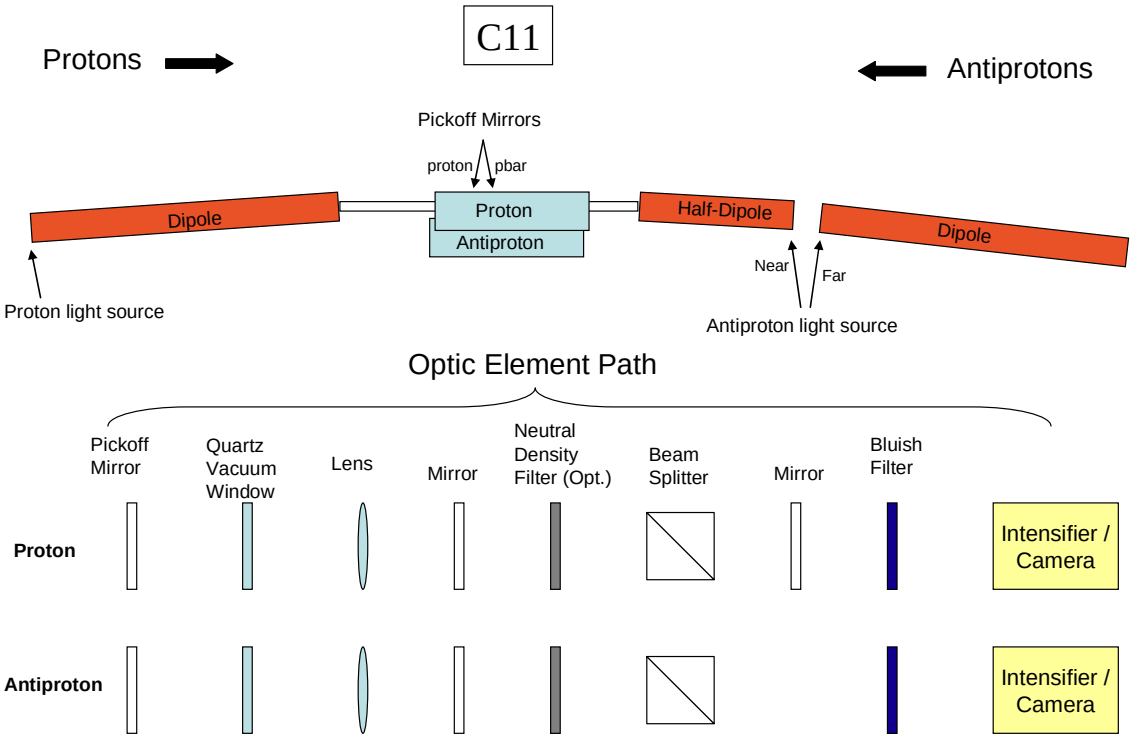

Proton System	
Distance from light source to pickoff mirror	746.5 cm
Distance from pickoff mirror to lens	22.9 cm
Distance from lens to camera	187.3 cm
Antiproton System	
Distance from near light source to pickoff mirror	472.2 cm
Distance from far light source to pickoff mirror	512.7 cm
Distance from pickoff mirror to lens	30.8 cm
Distance from lens to camera (near source)	84.8 cm
Distance from lens to camera (far source)	*83.8* cm

Figure 6: Overview of Synclite layout at C11. The pbar box does not have a second mirror. Table lists relevant distances for determining optical gain. There is only one magnet on the proton side, hence there is only one light source. There are 2 magnet edges on the antiproton side, thus there are 2 light sources. The system nominally looks at the Near source.

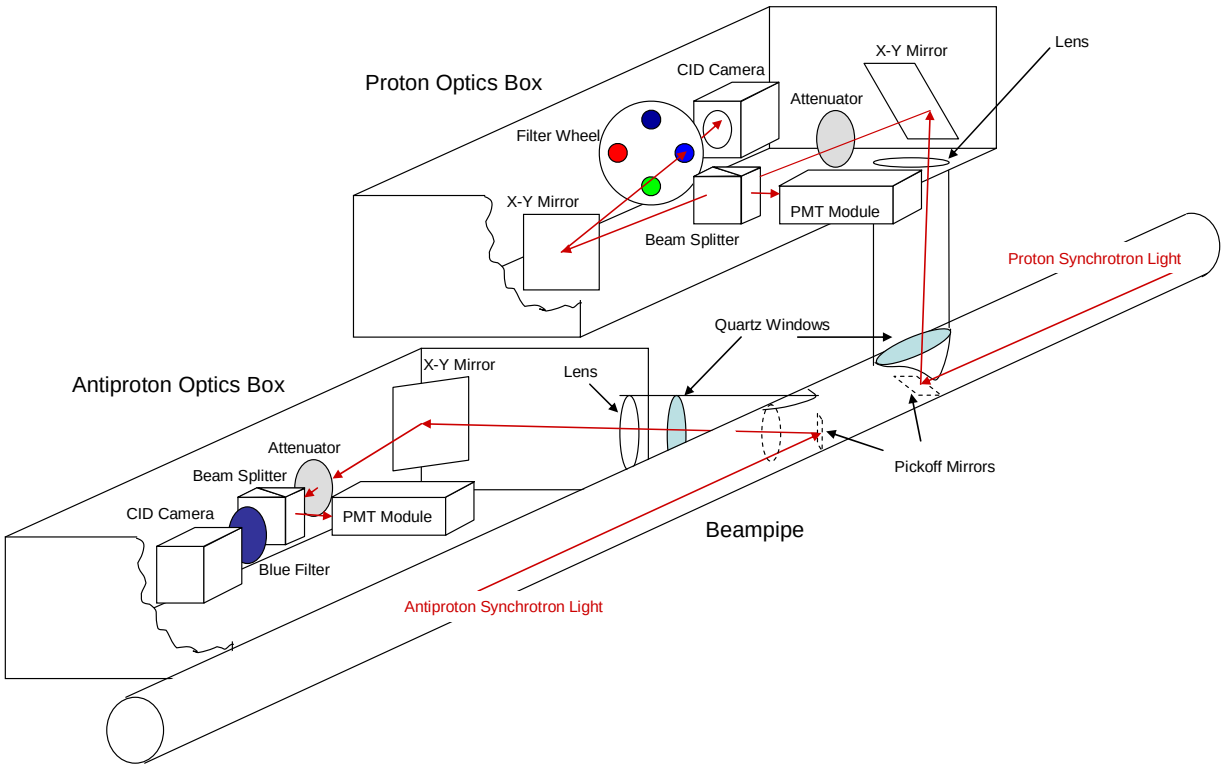

Figure 7: 3D view of Synclite systems.

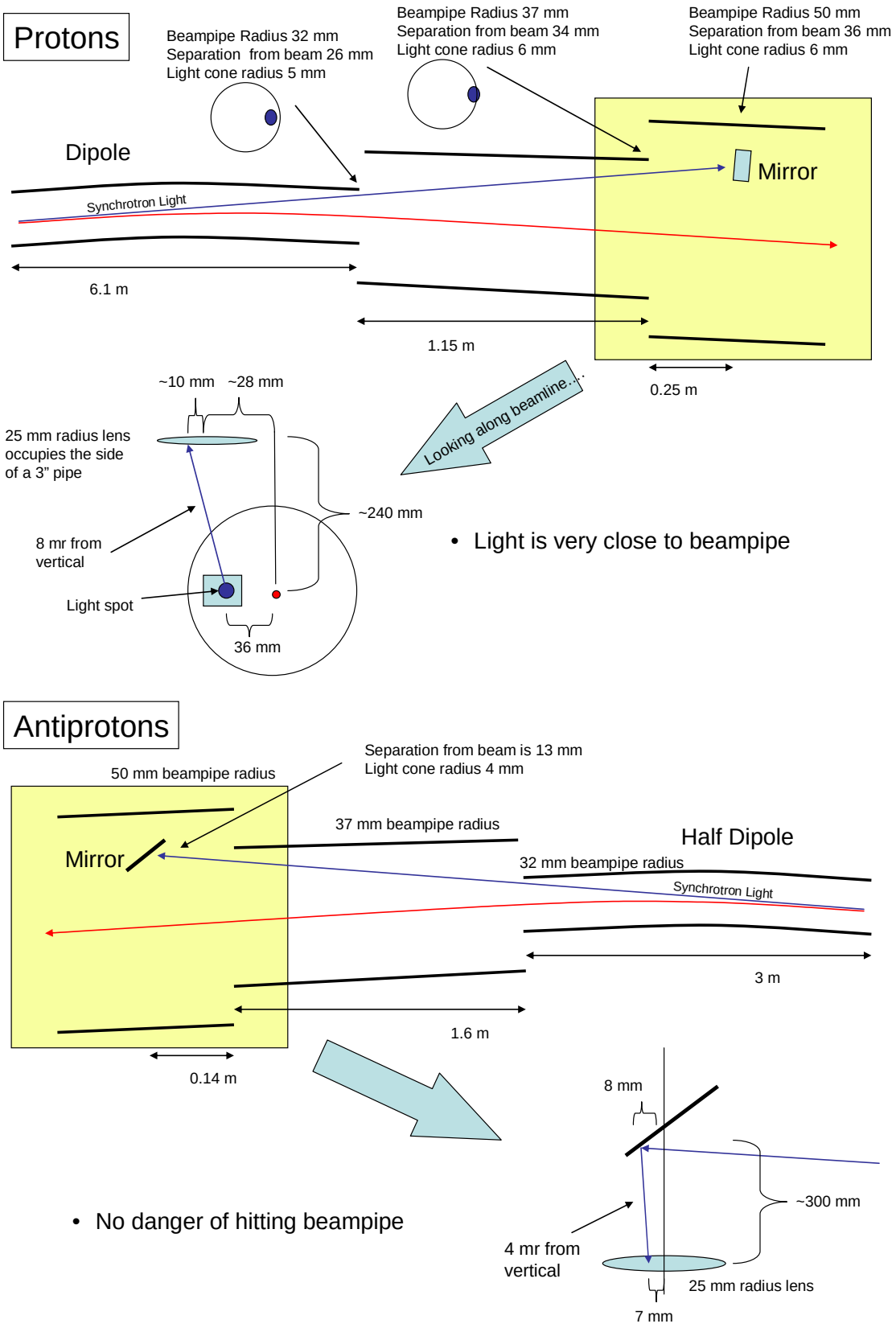

Figure 8: Details of beamline apertures and sizes, and where the light is relative to various optical elements. Despite the fact that it appears as though some fraction of the proton light should be lost, the simulation seems to indicate that there is no loss (see Section 4.2.1 regarding mirror moving study).

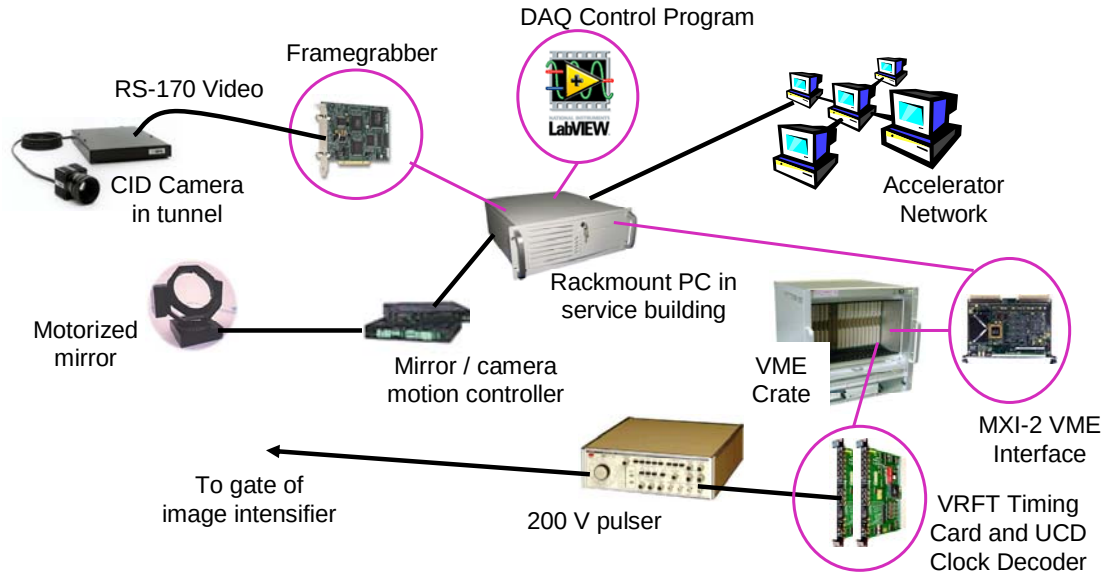

Figure 9: Synclite data acquisition system. The CID camera is attached to the output side of an image intensifier.

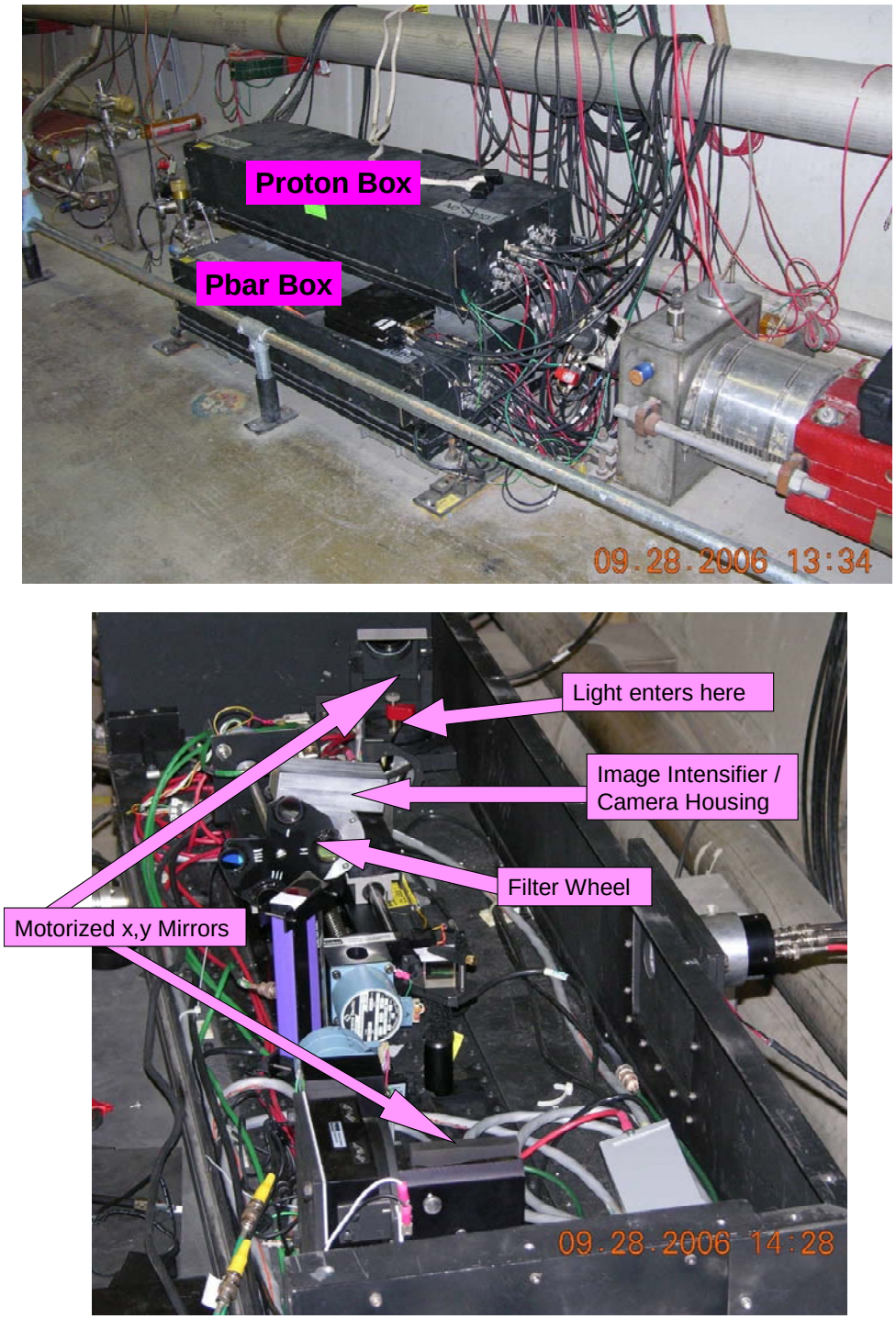

Figure 10: Top: C11 photo showing Synclite boxes. Bottom: Inside view of proton Synclite box.

Table 1 lists the expected number of photons after each optical element assuming bunch sizes of 250 x 10^9 for protons and 100 x 10^9 for antiprotons.

After object…	Object Efficiency		# of photons / bunch / 25 nm	
			Protons	Antiprotons
Magnet Edge	—		750,000	750,000
Pickoff Mirror	90%		675,000	675,000
Vacuum Window	90%		608,000	608,000
Lens	93%		565,000	565,000
x-y Mirror	90%		509,000	509,000
Beam Splitter	44%		224,000	224,000
x-y Mirror (proton only)	90%		202,000	—
Wavelength Filter	10 nm 40%	40 nm 160%	81,000	358,000
Photocathode	14%		11,000 p.e.	50,000 p.e.

Table 1: List of optical elements, their efficiencies, and the expected number of photons after the device for typical bunch sizes (250 x 10^9 protons, and 100 x 10^9 antiprotons). The last row lists the number of photoelectrons coming from the photocathode of the image intensifier. The fact that the starting number is the same for both protons and antiprotons is purely coincidence.

4 Calibration and Studies

Calibrations begin with studies of the readout electronics, namely, the image intensifier, CID camera, and PCI based framegrabber. Once the amplification and digitization process is understood, the locations of the components of the optical network are determined and the overall optical behavior of the system is studied by moving the pickoff mirrors and cameras and comparing the image profiles to the simulated ones from SRW. Finally, the distance scale is checked by comparing the motion of the beam as measured by Synclite with that measured by the Beam Position Monitors.

4.1 Intensifier and CID Camera

To accurately measure the beam shape, one must understand the response function of the readout system. In this case, that begins with the intensifier setup. Various studies were performed on this system, with most of them checking the dependence of the measured sigma on the effect under study. All studies were done on the proton system without a wavelength filter using sigmas from the vertical profiles to avoid the horizontal profiles which are non-gaussian. In Synclite, a profile results from summing in the other dimension, i.e. the vertical profile results from summing the 2-D image horizontally and plotting the 1-D array that results.

4.1.1 Intensifier Gain Behavior

The first two studies simply demonstrate the linearity of the intensifier system and are not studies of the effects on sigma. Figure 11 shows the gain as a function of MCP voltage (the image intensifier contains a micro-channel plate PMT). The behavior is quite linear (in a logarithmic sense).

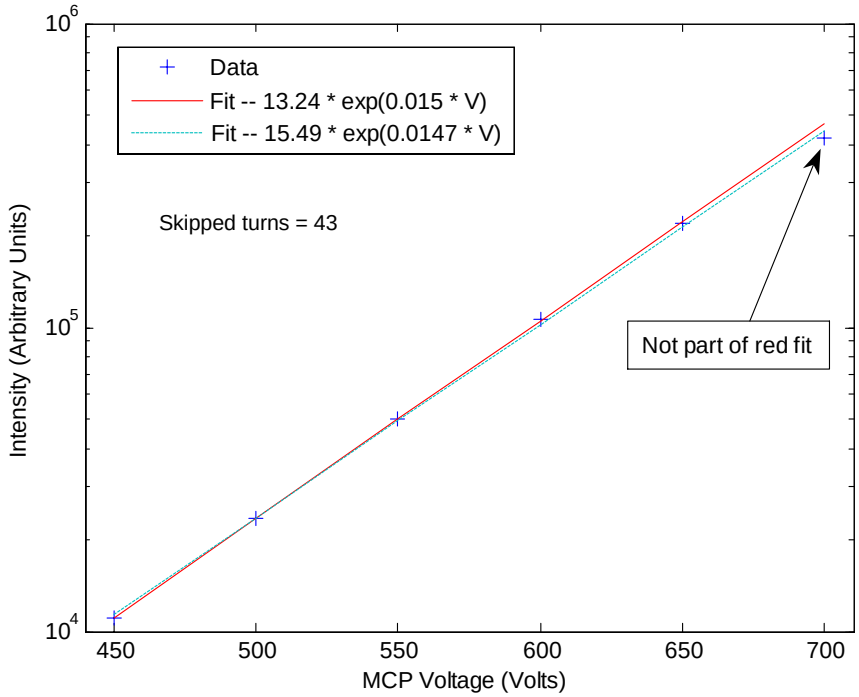

Figure 11: Intensifier gain versus MCP voltage. The fits are informational only. They are not used for any kind of correction. The largest voltage points may sag a bit due to camera distortion at large intensities. This is discussed below.

Figure 12 shows the linearity of intensifier gain with incident light. The nonlinearity is less than 5%.

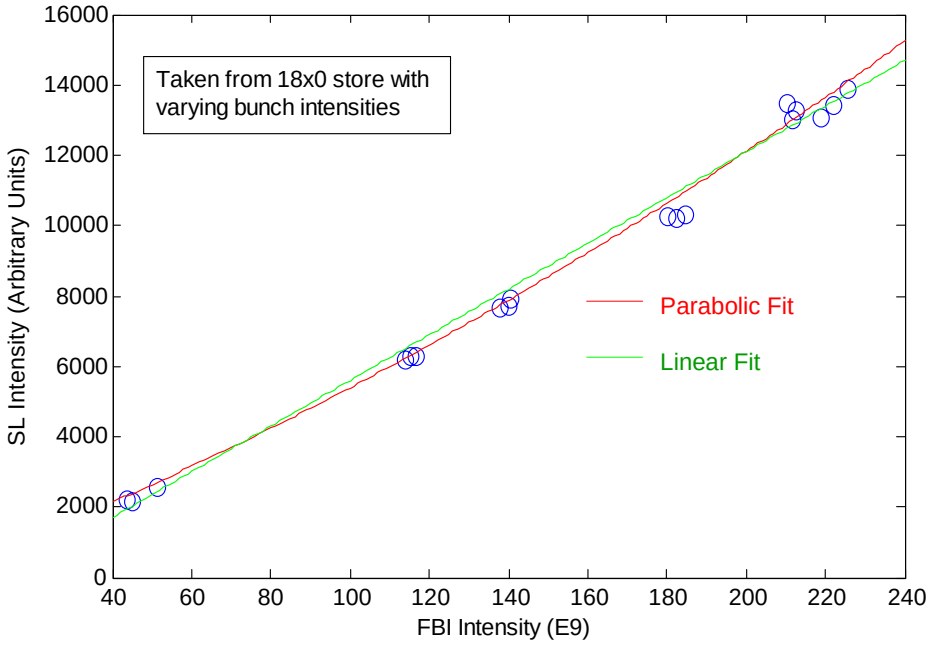

Figure 12: Synclite intensity versus FBI intensity for each bunch in a store with widely varying proton intensities. This serves to measure the nonlinearity of the gain which is less than ~5%.

4.1.2 Number of Framegrabber Frames

This refers to the number of camera image frames that are added together to form a final image from which measurements are made. While it would have been surprising to have seen an effect here, it was worth checking since most of the other studies make use of varying numbers of frames to improve measurement resolution. Figure 13 shows the dependence of measured sigma on the number of images in the fit. There is no effect greater than 0.2%.

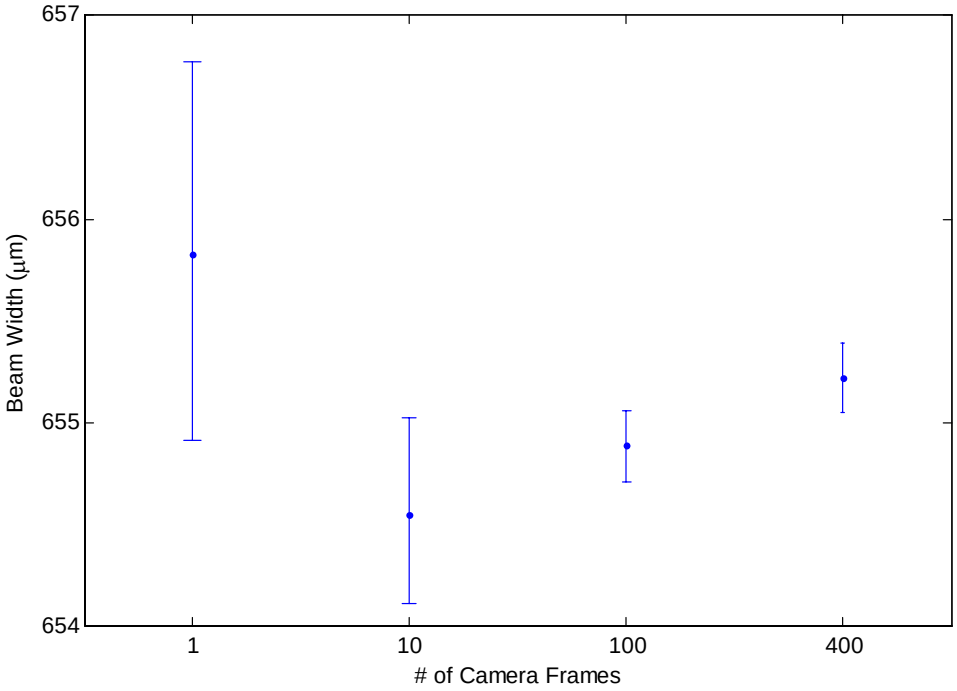

Figure 13: Dependence of measured sigma on the number of framegrabber frames added together in the fit. There is no effect greater than 1μm (~0.2%).

4.1.3 MCP Voltage and Gating Duty Cycle

Measurements are made of the vertical profile width as a function of the MCP voltage and the gating duty cycle (how many turns are skipped between each gate). Figure 14 shows the 3D results of this study. Figure 15 shows the same data but mapped to camera intensity. What this demonstrates is that the variation of sigma is strictly a function of total light coming off the phosphor screen of the intensifier. It is not a function of just voltage or just duty cycle. This effect is large enough to need a correction which is discussed later.

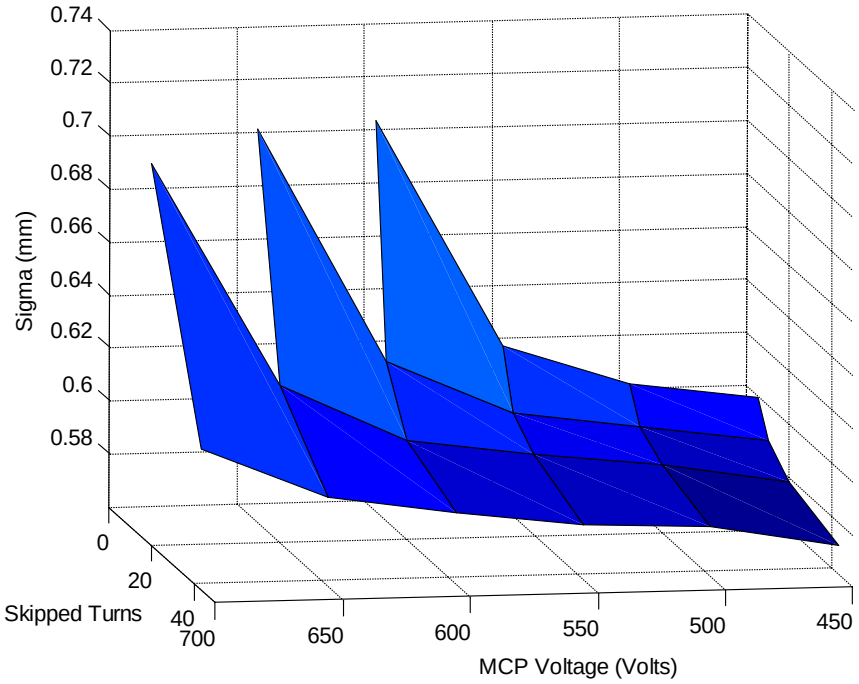

Figure 14: Variation of sigma with both MCP voltage and gating duty cycle. Skipped Turns is inverse duty cycle. It is the number of turns between gates. Distortions are seen as the amount of light hitting the camera increases. The amount of light increases both with increasing MCP voltage and with larger duty cycle (smaller skipped turns).

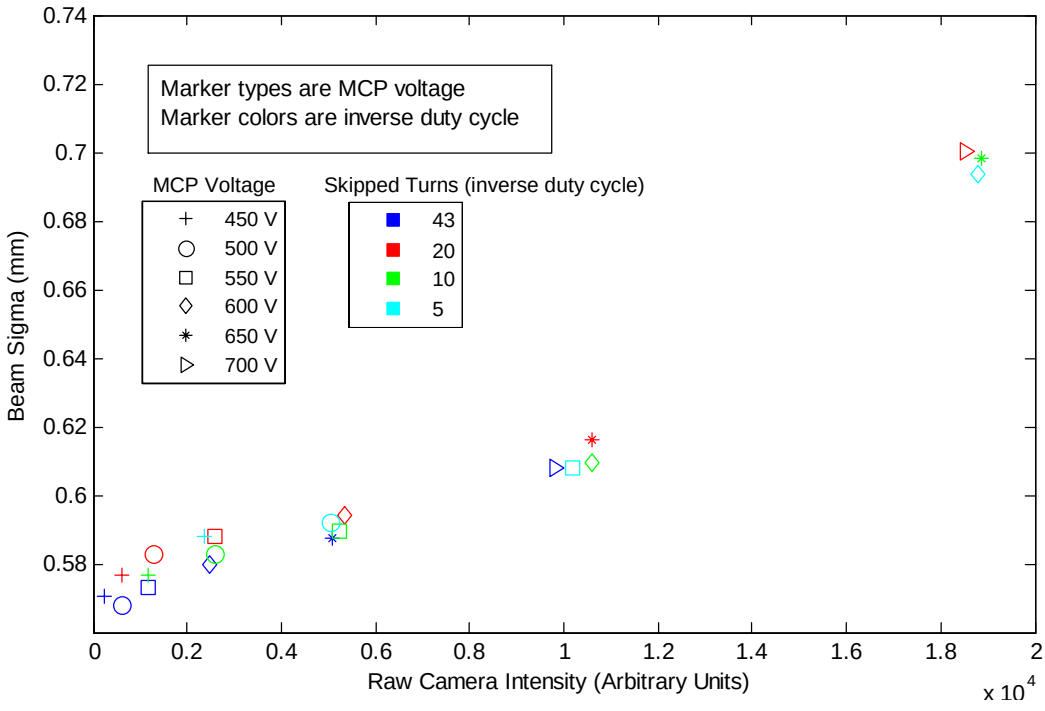

Figure 15: Variation of sigma with camera intensity. This plot contains all the points of the previous plot. Here they are expressed in terms of camera intensity and are symbol / color coded by voltage and skipped turns.

4.1.4 Incident Light

Figure 16 is the same plot as Figure 15 but with two more points overlaid on it. The two points are with the 4.2% optical attenuator in and out. As one can see, there is no additional dependence on incident light.

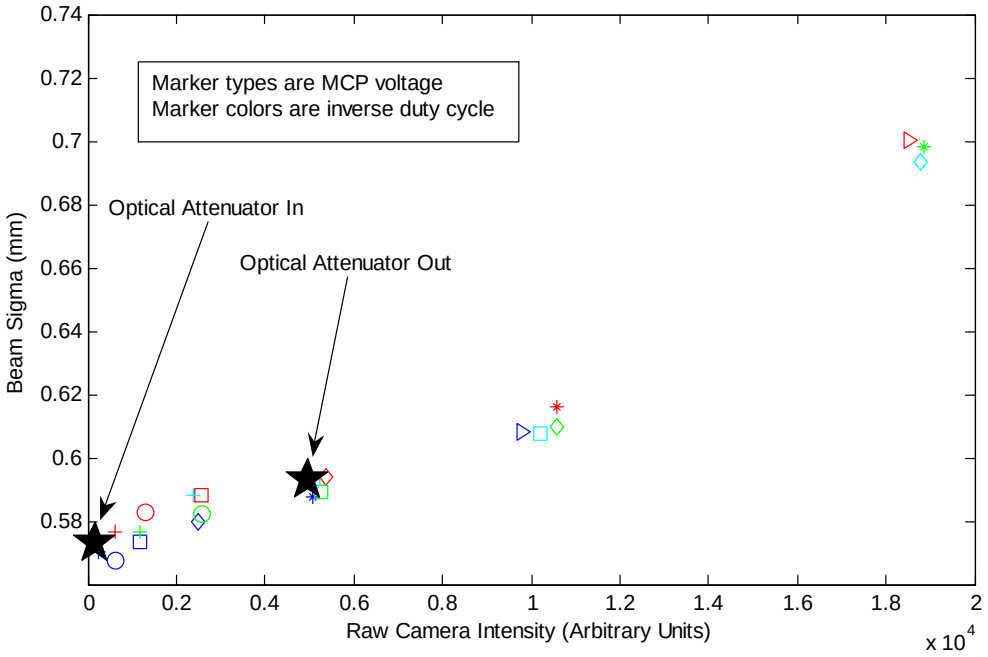

Figure 16: Same plot as above but with 2 more points. The dark stars show the effect of putting in the optical attenuator (neutral density filter). The difference in sigma is consistent with the difference in intensity.

4.1.5 Gating Voltage

The image intensifier is operated in a gated mode whereby the photocathode's voltage is switched between +30 V (off) and -150 V (on). Figure 17 shows the variation of sigma with pulsing voltage. The variation is consistent with what is expected if one considers just the intensity variation over the range of pulsing voltage.

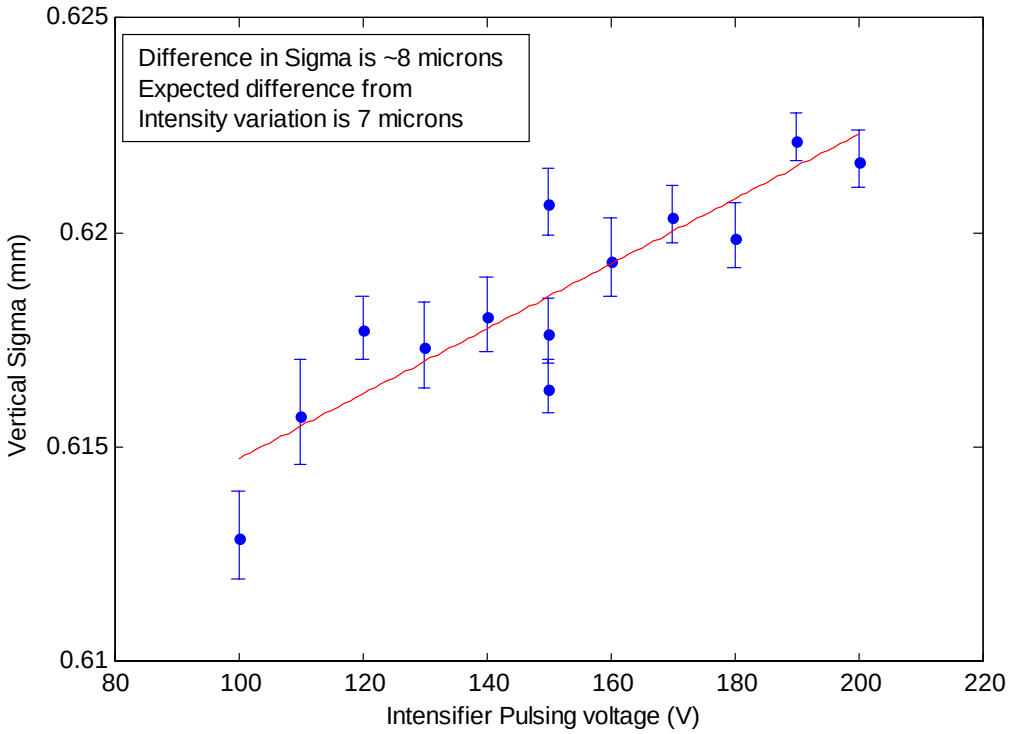

Figure 17: Variation in sigma with pulsing voltage. The variation is consistent with what is expected from the intensity variations which are a linear function of pulsing voltage. Thus there is no additional effect from this.

4.1.6 Position of image on Intensifier

If the image is moved around on the photocathode, the measured sigma varies. The image position is changed by moving one of the mirrors in the Synclite box. Figure 18 shows the variation of antiproton sigma with the horizontal and vertical positions of the image. The histograms of these sigmas are displayed in Figure 19 and have widths of a few percent.

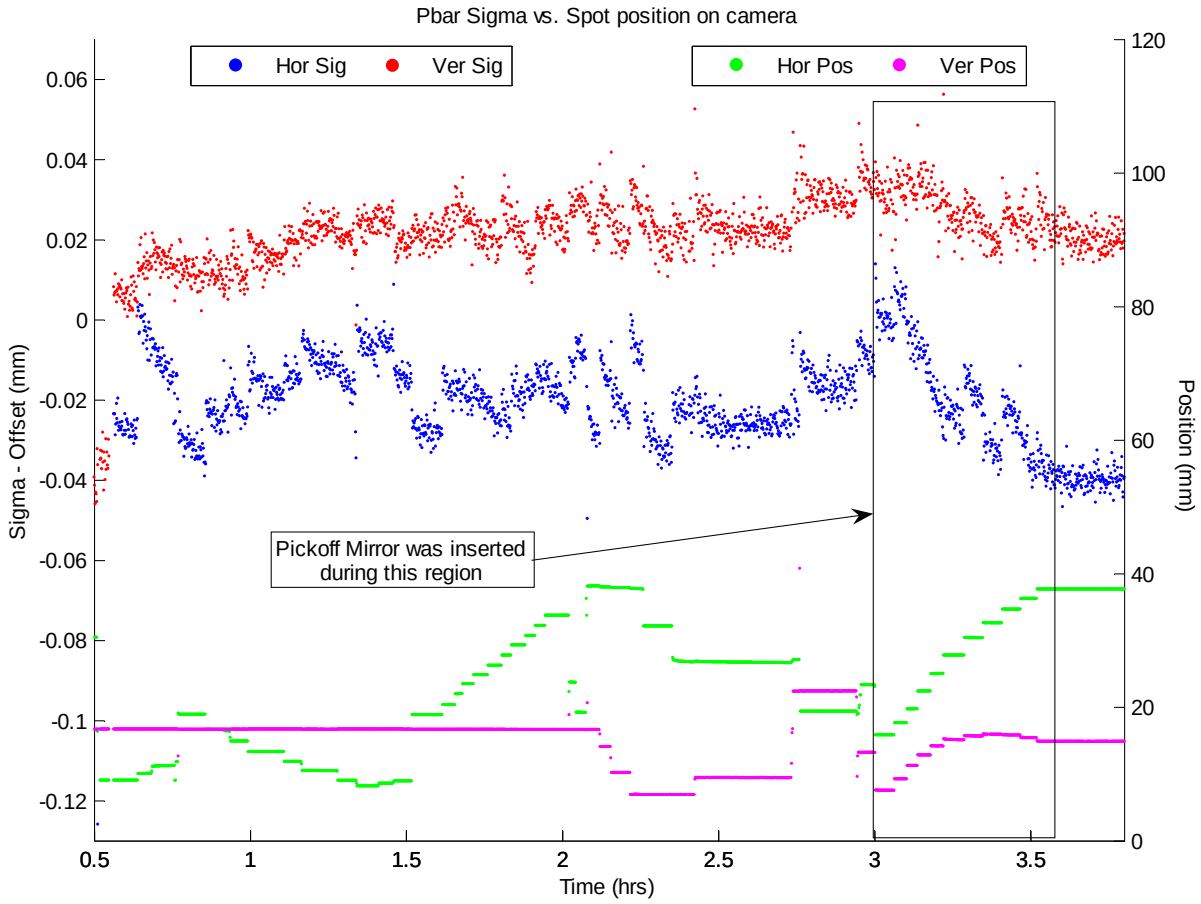

Figure 18: Variation of antiproton sigma as the spot is moved around on the camera using one of the mirrors in the Synclite box. The box indicates the region where the pickoff mirror was inserted by 30 mils in steps of 3 mils. The sigma data has had its offset subtracted to enable everything to be displayed on one plot. The average horizontal(vertical) sigma is ~0.5(0.7) mm.

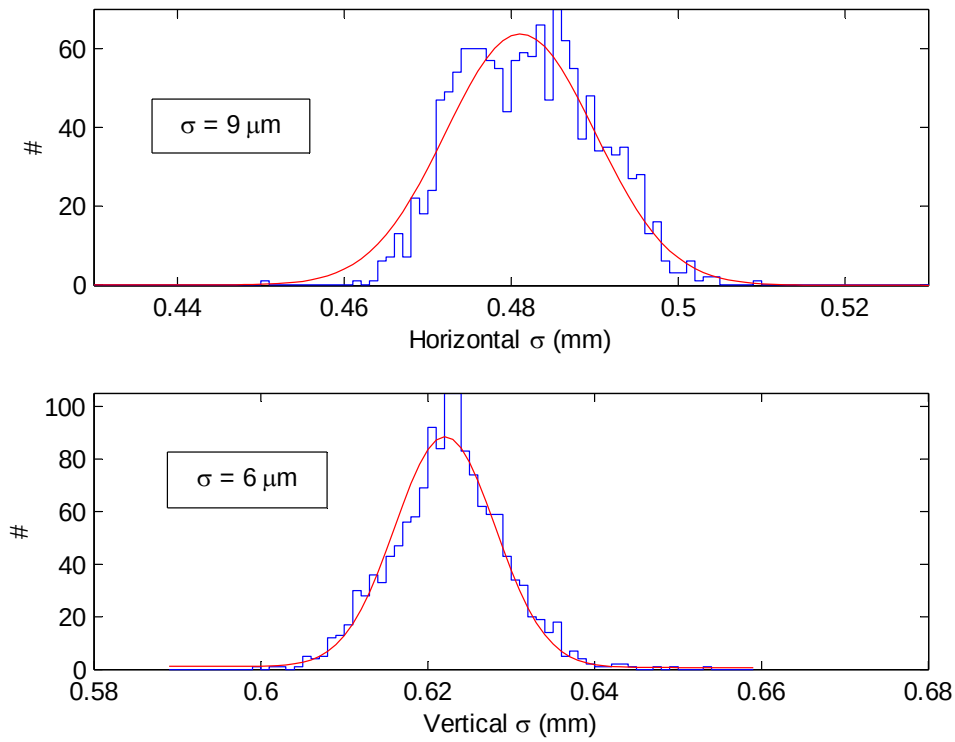

Figure 19: Distribution of antiproton sigmas as the image is moved on the intensifier face.

4.1.7 Miscellaneous

4.1.7.1 Differences Between Proton and Pbar Intensities

During the 2005 shutdown, new CID cameras were installed and an image intensifier was swapped to arrive at two similar systems. The intensifiers were chosen such that the factory measured gains were nearly the same and since the cameras and controllers are the same model, the expectation is that they should have similar gains. The differences in the optical systems at that time are summarized in the following table.

Element	**Proton / Antiproton**
Beam Splitter	50%
Mirror	90%
Bandpass Filter	25%
One dipole edge	40%
Total	**4.5%**

Table 2: Fraction of light the proton Synclite system sees relative to the antiproton system for each extra element or shortcoming that the proton system has.

The final analysis obtains a ratio of proton to antiproton of 1.7, or 70% more light in the proton system. This is probably acceptable given the assumptions made about the camera systems and such.

4.1.8 Corrections

4.1.8.1 Intensifier and Camera System

The present cameras exhibit similar behavior to previous cameras, except for seemingly more consistency. What is needed for this is to determine the image sigma transfer function, *i.e.* what is the fit sigma for a given sigma in. Figure 20 shows the variation of sigma with framegrabber intensity. This data was taken during a normal store but with the skipped frames controlled manually to fully scan the intensity range. Sigmas at low intensities are difficult to measure. As such, one can normalize the measured sigmas to an intensity of 250 counts. And then subtract off in quadrature a value determined by flattening the emittance ratio between Synclite and the Flying Wires for instance. A better approach might be to measure the response function of the camera system as a function of intensity using a calibrated photodiode. This may be attempted at some point.

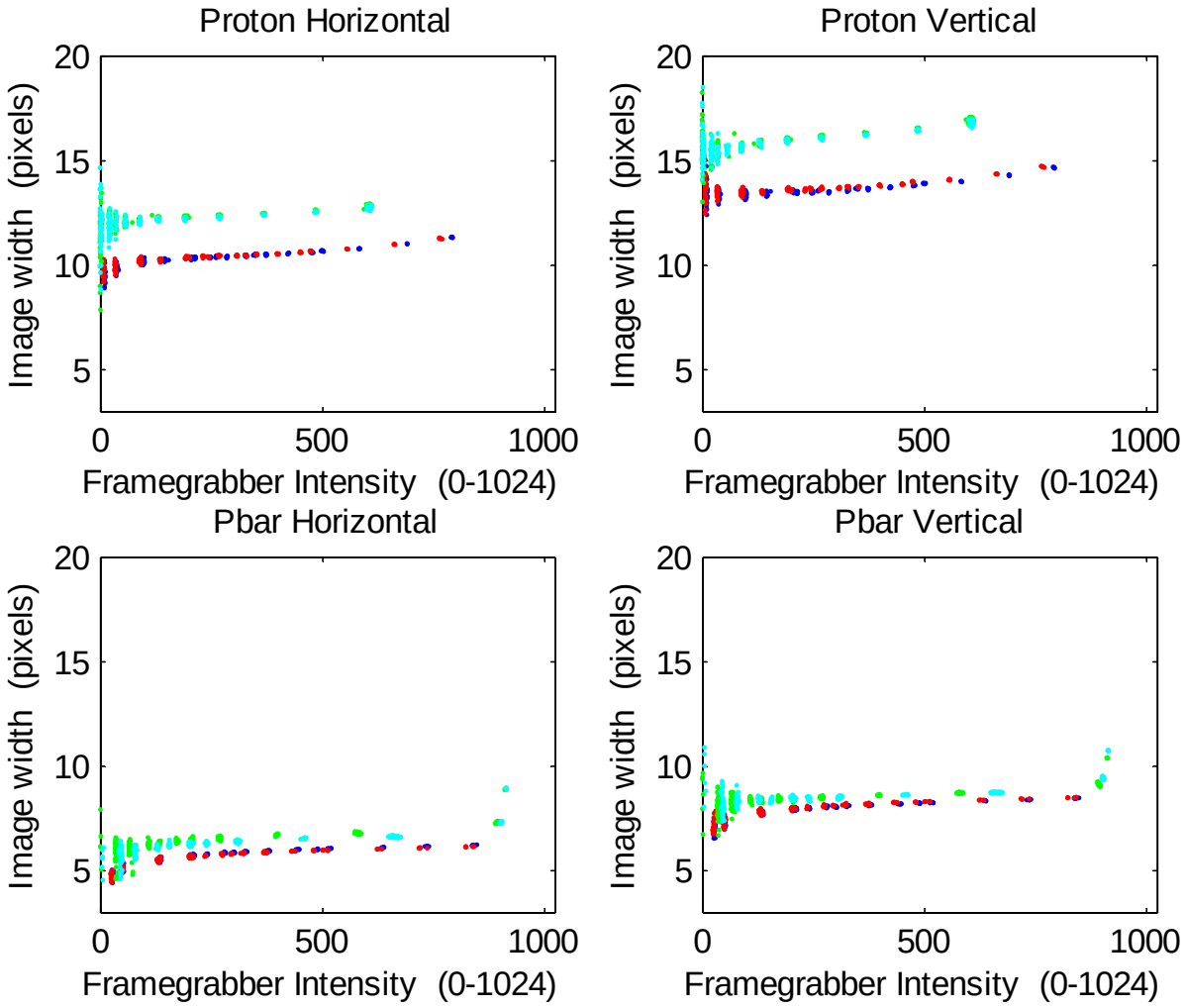

Figure 20: Variation of measured sigma with intensity.

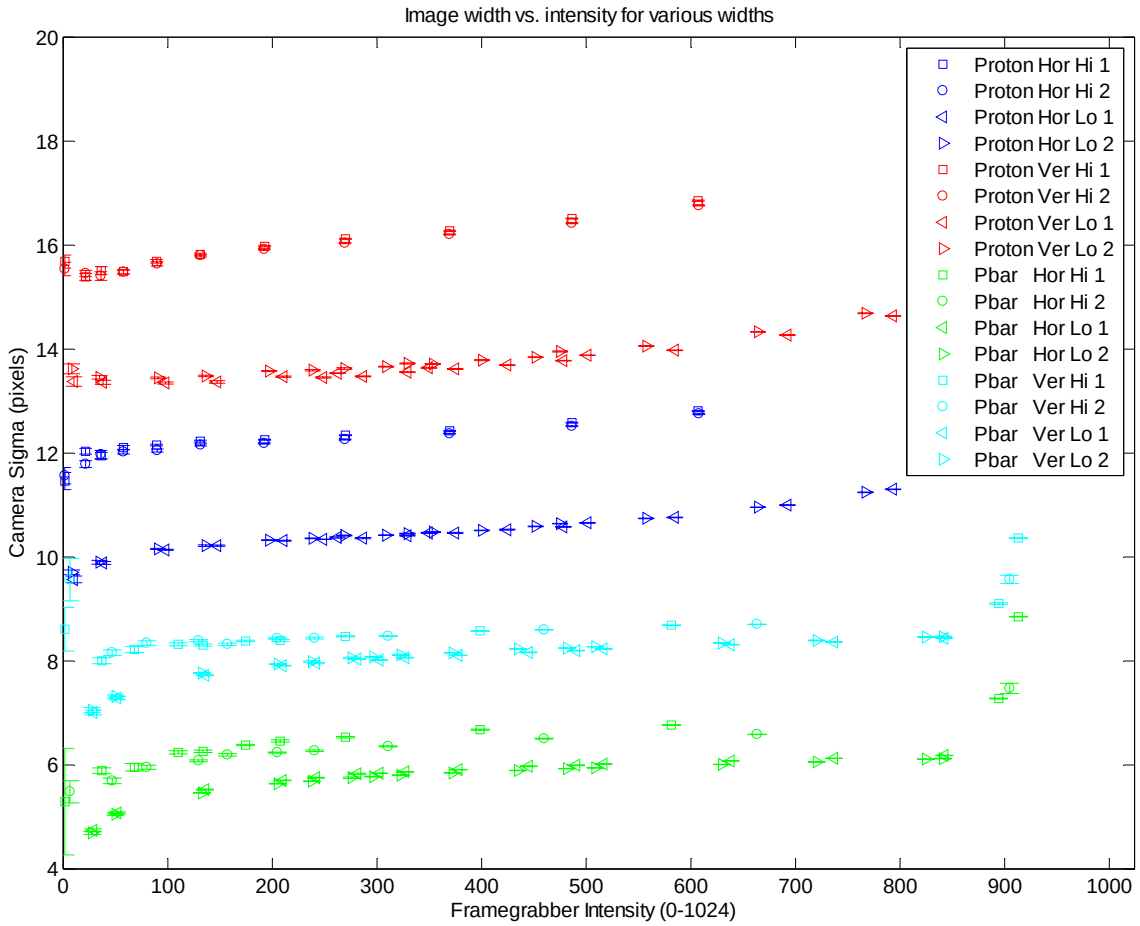

Figure 21: The data points here are the result of clustering the previous plots.

Figures 21 and 22 show the same data as Figure 20 after a clustering algorithm was run on it. The latter has the fitted lines that are used to correct the sigmas back to the value at an intensity of 250 counts. Figure 23 is a parameterization of the variation in slope as a function of fitted sigma. This behavior is entirely expected based on a generic non-linear response model where the measured intensity in any given pixel is less than the actual intensity by an ever increasing amount as the actual intensity is increased. In equation form, this would be something like

$$I_{response} = I_{actual} \cdot (1 - kI_{actual}) \qquad \textbf{(1)}$$

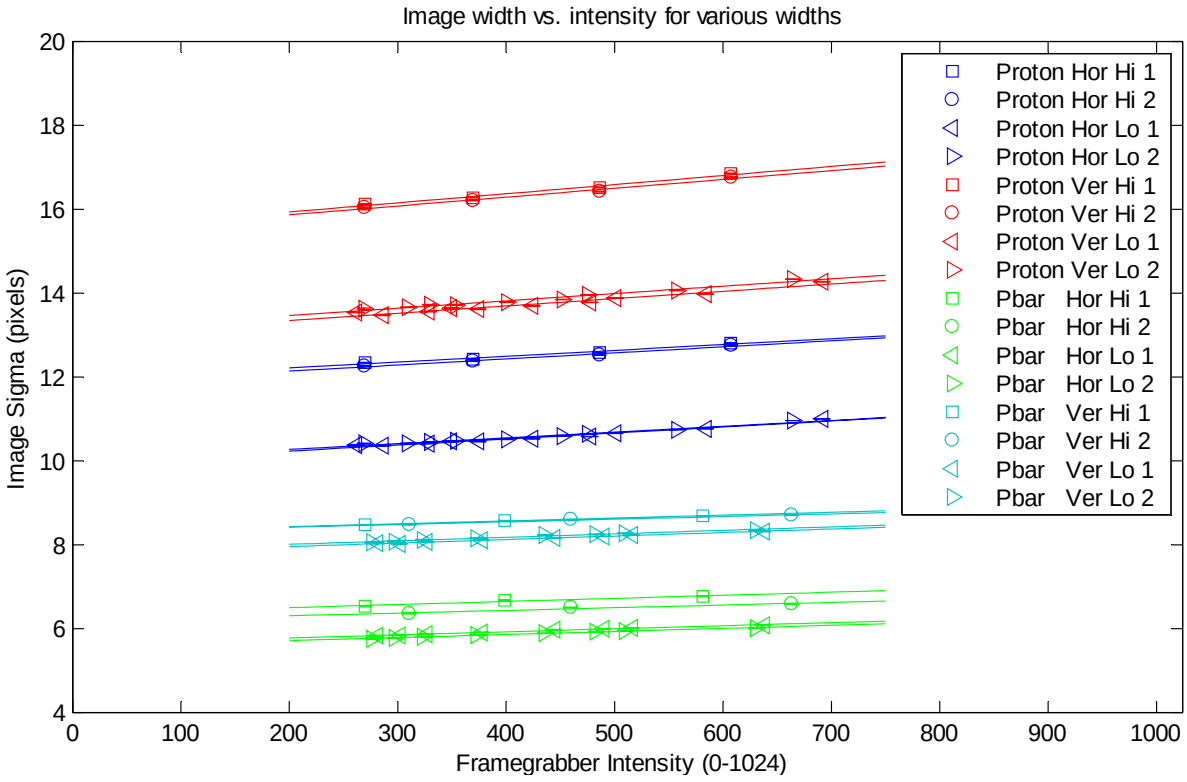

Figure 22: Variation of image width with intensity.

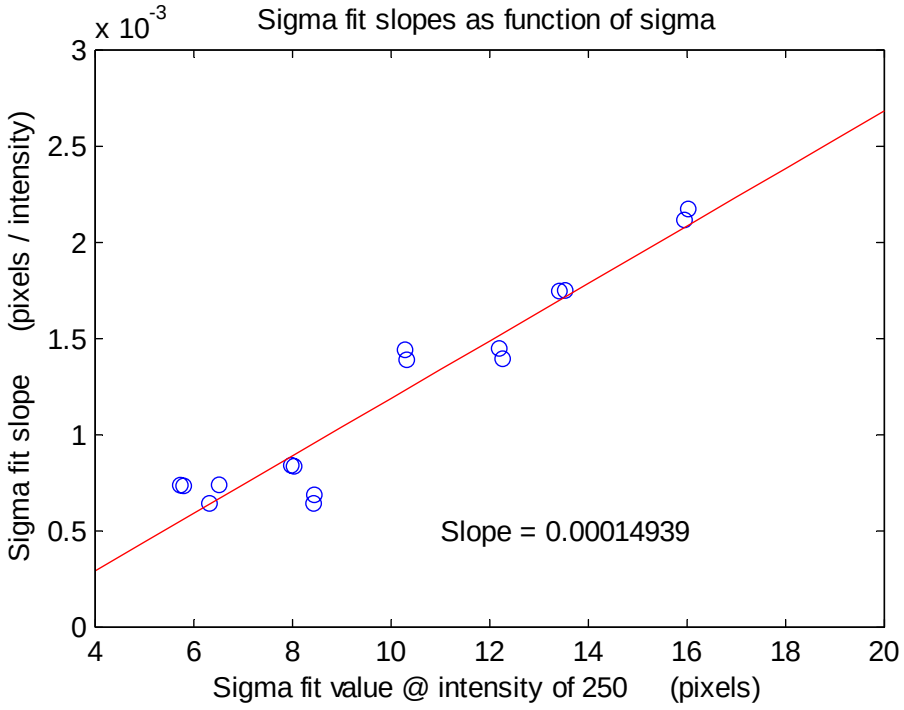

Figure 23: Variation of correction slope with sigma at an intensity of 250. The intercept is -0.00032756.

The corrected sigma at an intensity of 250 counts is thus

$$\sigma_{250} = \left[\frac{\sigma_m + 3.28\times10^{-4}(I-250)}{1+1.49\times10^{-4}(I-250)} \right] \quad \textbf{(2)}$$

where σ is the true sigma, σ_m is the measured sigma, and I is the peak camera intensity.

4.2 Optical Network

The positions of elements in the optical network were measured and are diagrammed in Figures 24 and 25. Figure 26 shows the magnetic field strength at the end of a dipole magnet as a function of longitudinal position. This information is used to determine the distances from the lens to the camera, and from the lens to the effective object, which is taken to be the half-field point of the dipole.

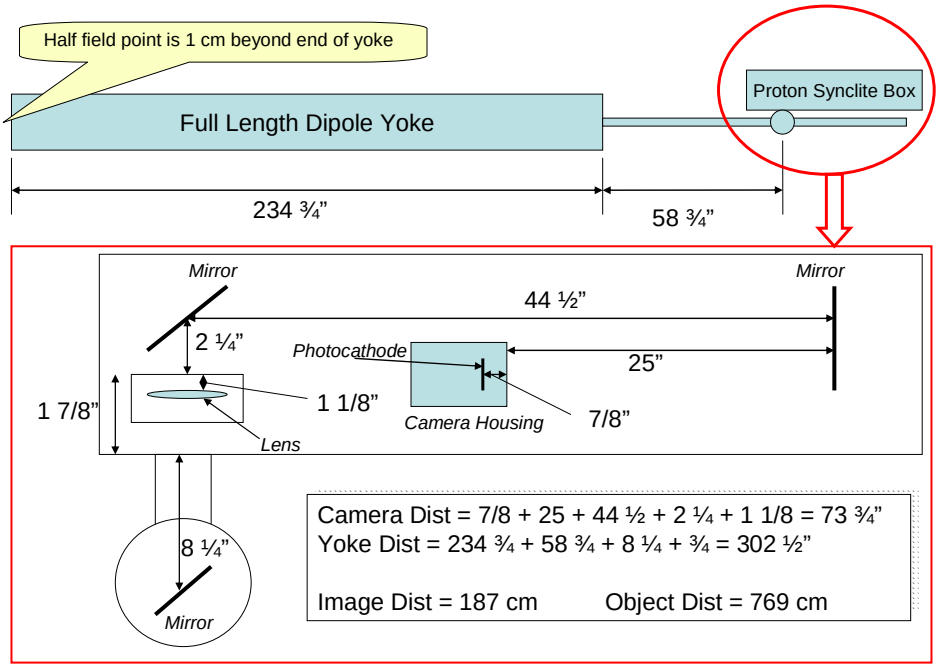

Figure 24: Proton optical distances as of January 2006. This view is looking at the side of the beam line and device. The Object Dist value has 1 cm added for the extension of the magnetic field beyond the yoke (see Figure 26).

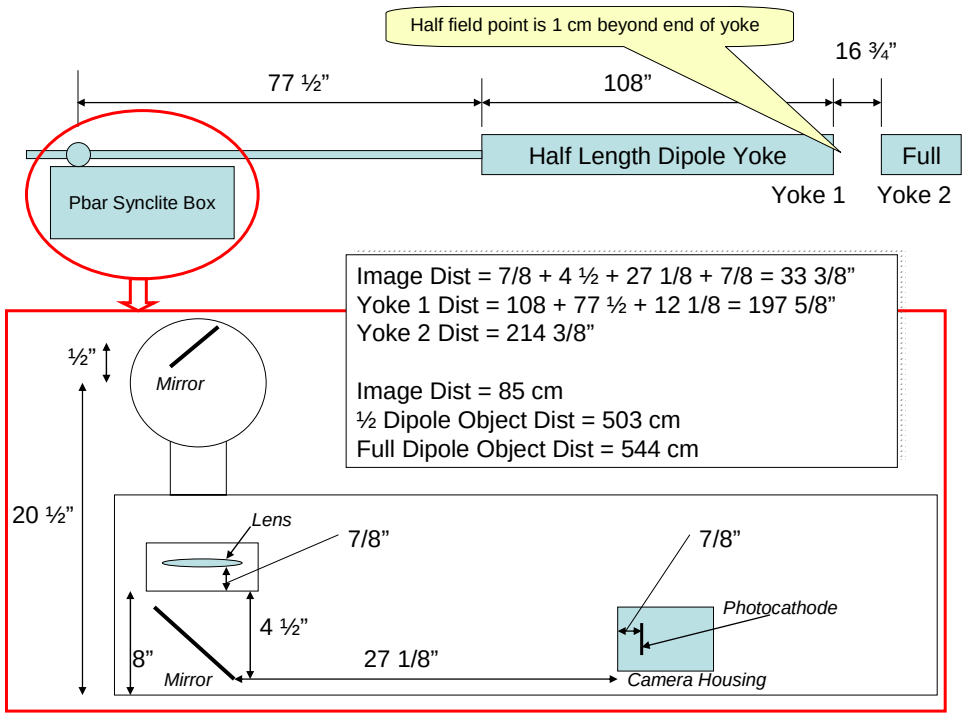

Figure 25: Antiproton optical distances as of January 2006. This view is looking down on top of the beamline and device. The Object Dist values have 1 cm added for the extension of the magnetic fields beyond the yokes (see Figure 26).

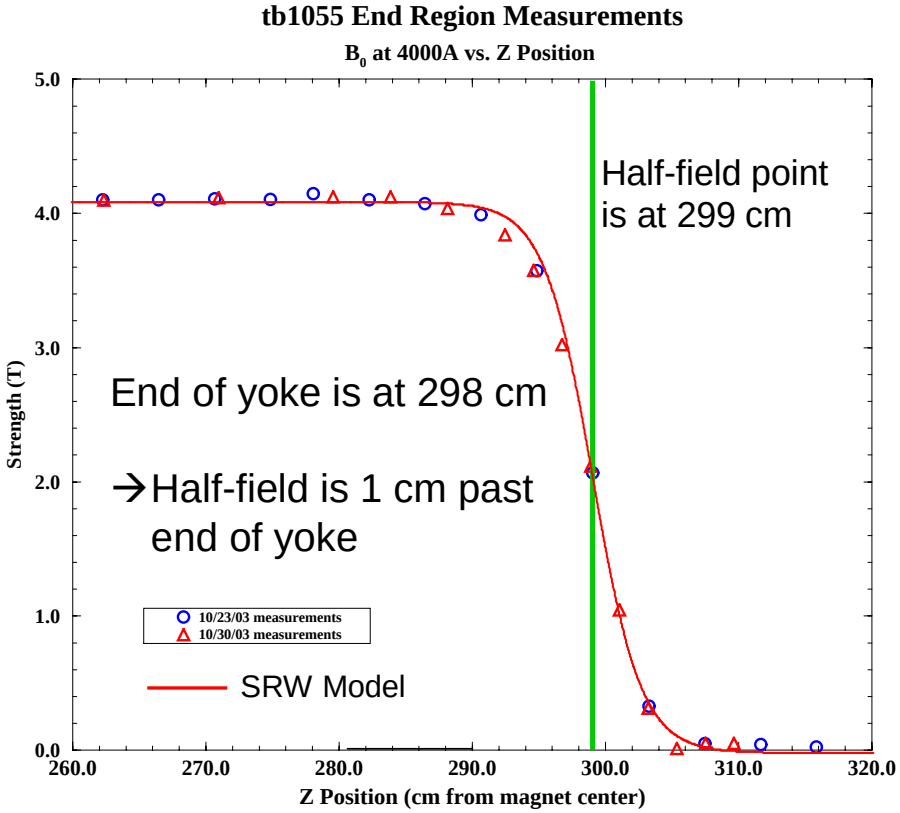

Figure 26: Location of half-field point with respect to the end of the yoke of a TeV dipole magnet. This plot was obtained from Phil Schlabach in Technical Division. The SRW model is superimposed on the magnet data.

Studying the optical network involves a number of items, such as moving the pickoff mirror to change the ratio of body to edge light, moving the camera focus, and verifying the wavelength dependence of the images. All these studies are compared to calculations run in SRW. When using SRW to do wavelength dependent studies, the focal length of the lens must be adjusted for the wavelength of interest. Figure 27 shows the behavior of the proton focal length as a function of wavelength for the BK7 glass in the lens. Equations (3) and (4) are the proton and antiproton focal lengths as functions of wavelength (wavelength is in units of Angstroms).

$$f_{proton} = (-2.8921\times10^{-9})\lambda^2 + (4.6847\times10^{-5})\lambda + 1.3245 \quad \text{meters} \qquad \textbf{(3)}$$

$$f_{antiproton} = (-1.446\times10^{-9})\lambda^2 + (2.3424\times10^{-5})\lambda + 0.6623 \quad \text{meters} \qquad \textbf{(4)}$$

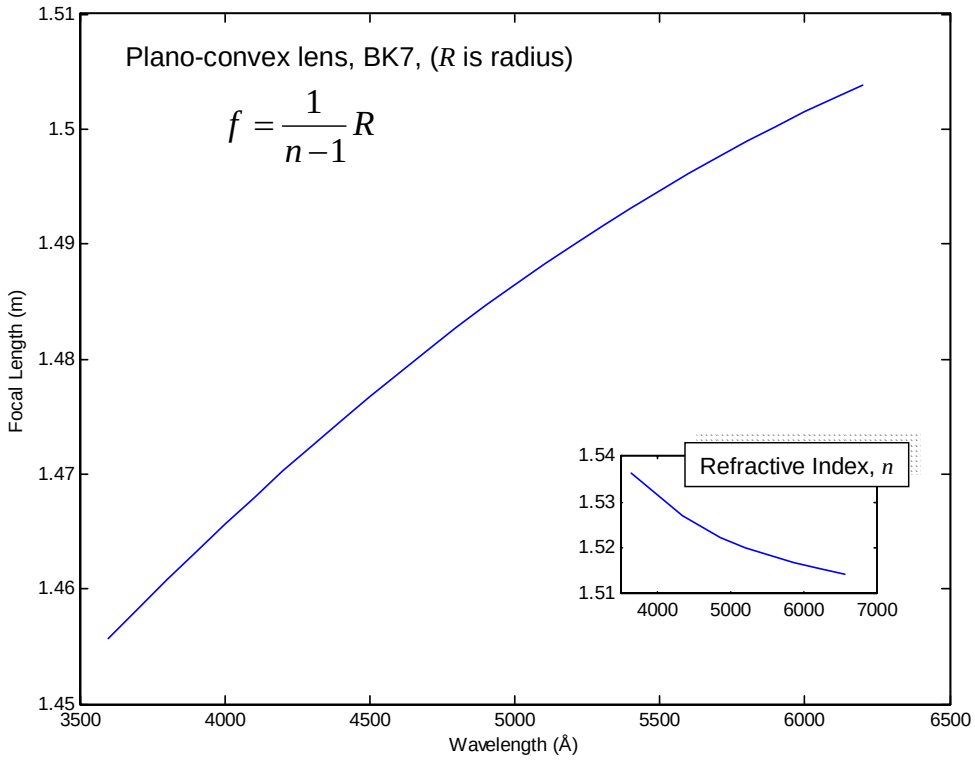

Figure 27: The inset plot shows the wavelength dependence of the index of refraction of BK7 glass (of which the lens is composed). The main plot shows the dependence of the proton lens focal length on wavelength.

4.2.1 Pickoff Mirror Motion

One way to study Synclite imaging is to move the pickoff mirrors in or out, thereby changing the ratio of edge light to body light picked up by the mirror. For the protons, the light is near the edge of the beampipe, therefore one can add more body light by moving the mirror in further, but cannot exclude the edge light since the mirror cannot be moved in far enough to do that. For the antiprotons, the edge light is much closer to the beam and therefore one can exclude the edge light altogether leaving just body light. Adding more body light in general produces a horizontal tail in the image. This can be understood qualitatively in Figure 28 where the light cones from different sections of the beam trajectory do not lie on top of one another. The height of the tails is determined by the relative amounts of edge and body light.

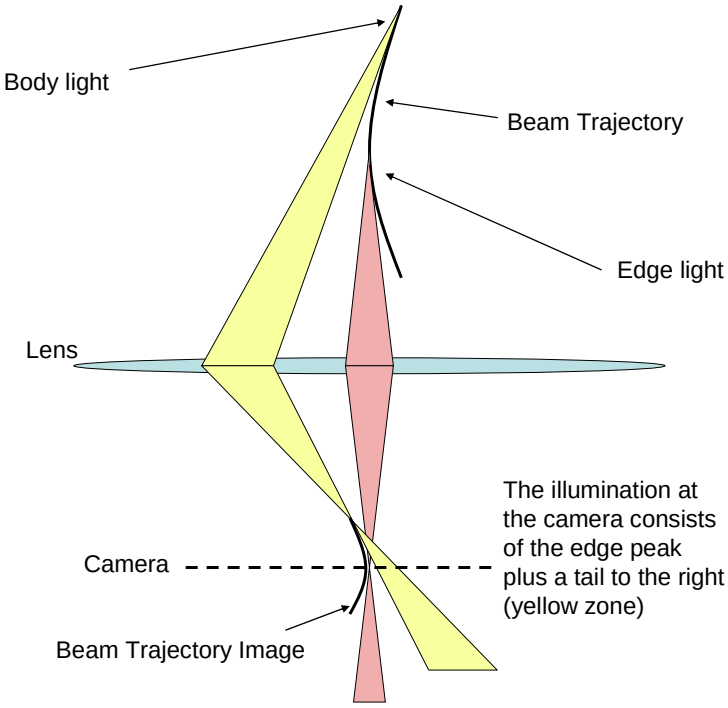

Figure 28: Cartoon diagram of contributions of edge and body light. In general, if one is focused on the edge, the body light contributes a tail since its light cone centroid is not in the same transverse location as the edge light cone.

Figures 29 and 30 show horizontal slices at different locations of the pickoff mirrors for protons and antiprotons. The numbers expressed as XXX mils[5] are relative to an arbitrary zero. That is to say they are used only for determining relative mirror positions (larger numbers mean further into the beam). The plots consist of data points and lines from SRW calculations.

For the protons, the inside edge of the mirror started at 1300 mils which is quite a distance into the beampipe. Each successive step moved the mirror further out with an accompanying decrease in both the amount of body light being intercepted and the length of the tails. The agreement with SRW is very good over the range of mirror positions.

For the antiprotons, the inside edge mirror started at 1060 mils which is close to the beampipe wall, and was moved progressively further into the beampipe. What is seen here is that the distributions increase slowly in size until the edge light is encountered, and the length of the tails increases as the mirror picks up a wider range of body light. Again, the data are in good agreement with SRW distributions.

[5] A mil is a thousandth of an inch, or 0.0254 mm.

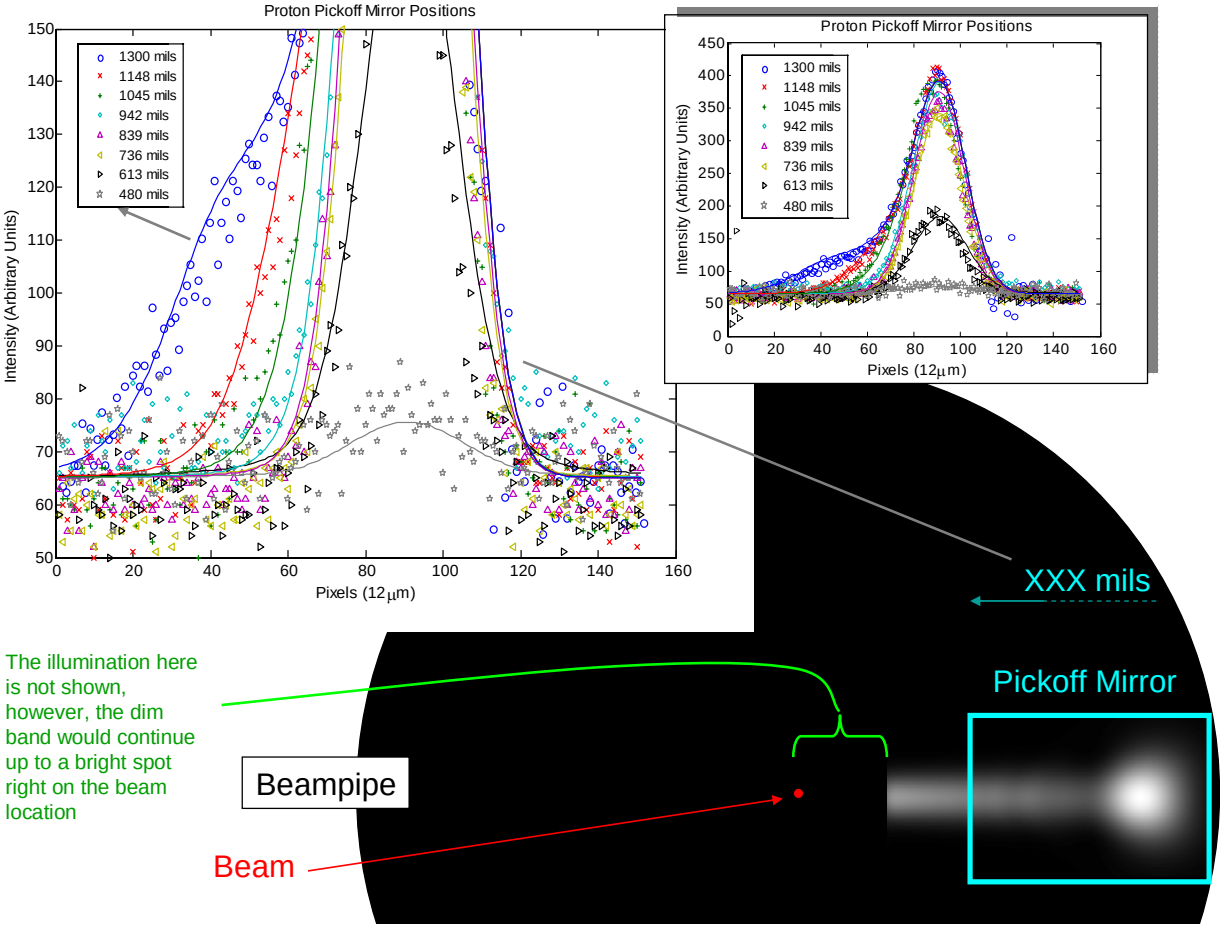

Figure 29: Diagram of proton pickoff mirror and synchrotron radiation in the beampipe. The drawing is not to scale. The number of mils represents only a relative position of the pickoff mirror for each step, i.e. it is not measured relative to the beampipe. For reference, the 480 mils position corresponds to the left edge of the mirror being positioned just to the right of the bright spot. The inset plot is the same plot as the large one, but shows the full height of the distributions. An important point to note on this plot is that the smallest distribution has a width about the same as the larger ones. The reason this is important is that it means the beampipe is not clipping the light. If it was, the beampipe and the mirror would act as a narrow slit and produce a very broad distribution.

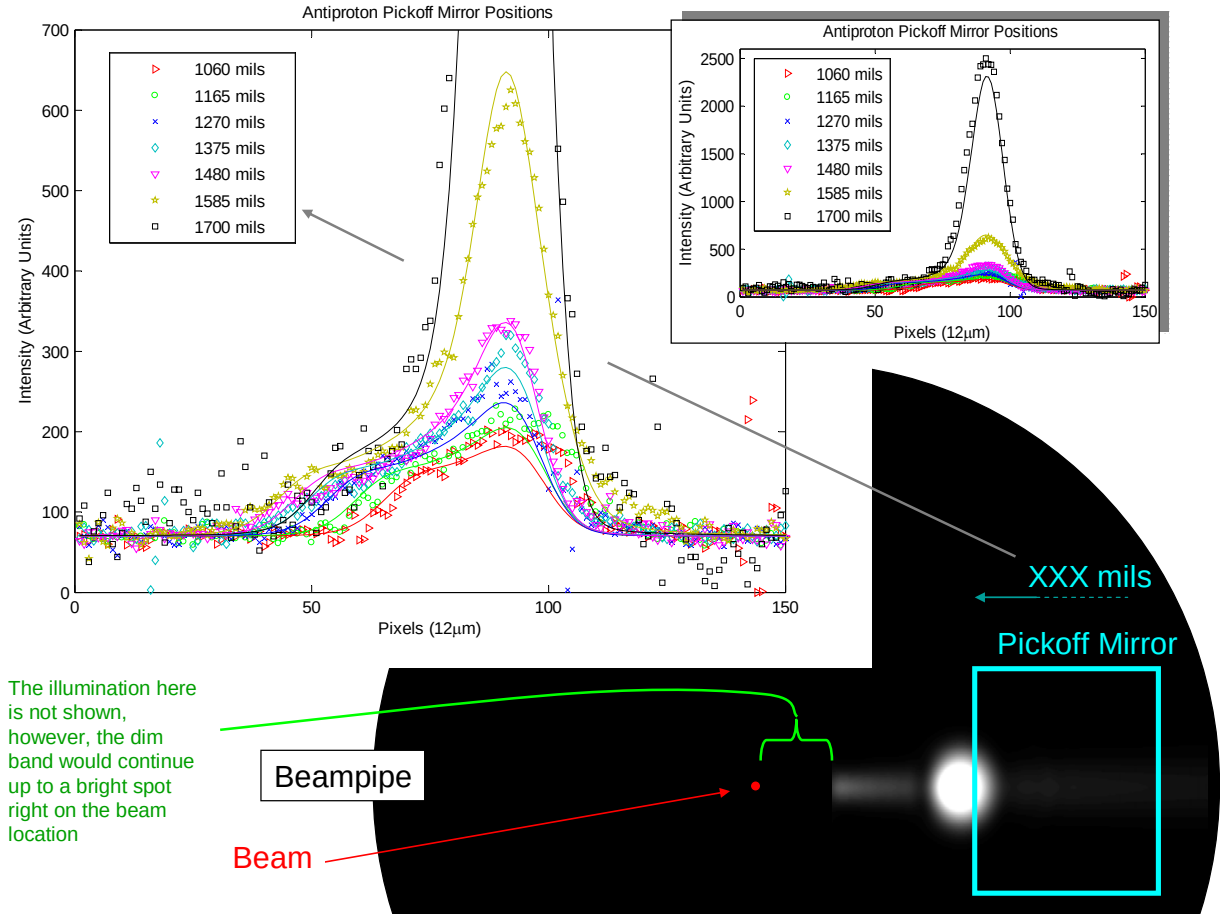

Figure 30: Diagram of antiproton pickoff mirror and synchrotron radiation in the beampipe. The drawing is not to scale. The number of mils represents only a relative position of the pickoff mirror for each step. It is not measured relative to the beampipe for instance. For reference, the 1700 mils position corresponds to the left edge of the mirror being positioned on the left edge of the light spot. The inset plot is the same plot as the large one, but shows the full height of the 1700 mils position.

Figures 31 and 32 demonstrate the sensitivity of the proton and antiproton SRW distributions to various parameters other than mirror position. As one can see, there is some flexibility in tweaking the shape of the distributions, but on the whole, they agree quite well.

It may occur to the reader when looking at these horizontal images, that either the proton or antiproton images are flipped horizontally. If that does occur to you, then relax, because you are quite correct. The plots were generated in the most convenient fashion which happened to have the antiproton image flipped horizontally.

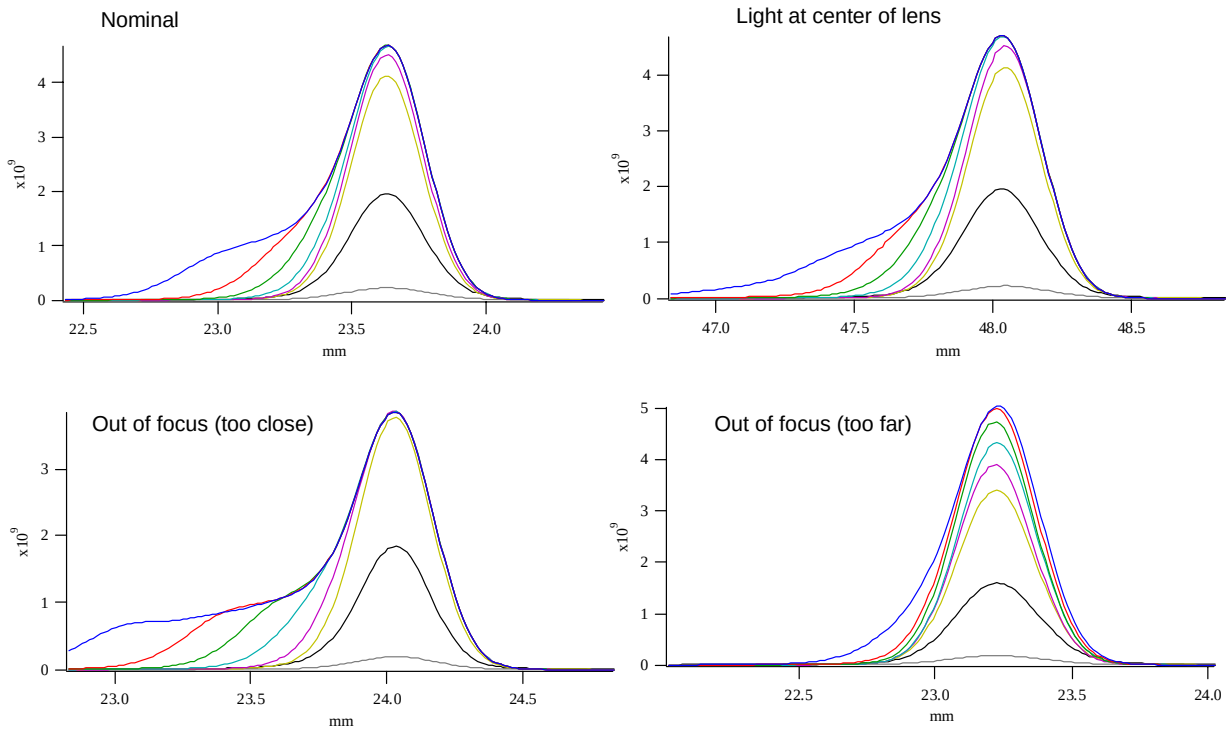

Figure 31: Proton simulations with different parameters. Notice the effects on the tails. The tail height doesn't change, but the extent of the tail does.

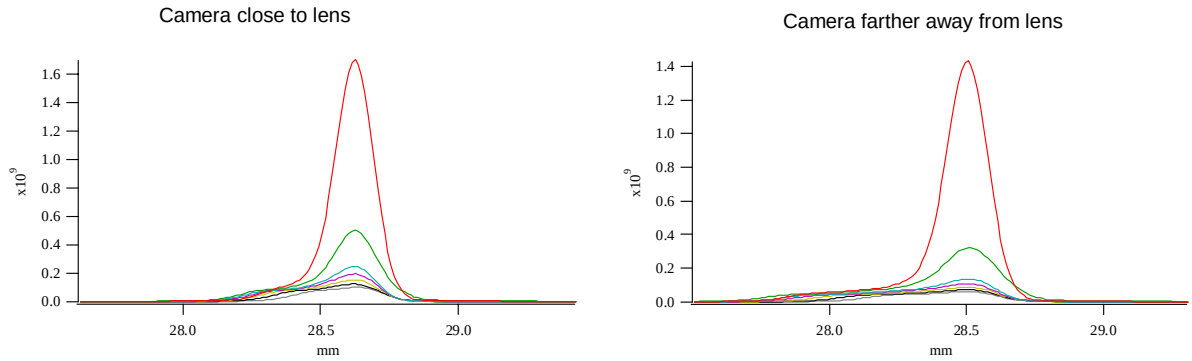

Figure 32: Antiproton simulations at two different camera positions. As with the protons, he camera position affects the extent of the tails but not the height.

On an historical note, after it was pointed out that the antiproton light may in fact be body light, the antiproton mirror was inserted further into the beampipe, and a sequence of images was observed that contained two peaks (Fig. 33). Speculation was that the second peak was either a reflection or the second magnet edge. Neither of these turned out to be correct. As was seen earlier in Figure 28, the contributions from the edge and the body can split since the centroids of the light cones follow different paths, and indeed, as Figure 33 shows, the simulation reproduces the double peak nature. The clear double peak is only present when the camera is focused on the body, which was the case when it was first inserted. If the camera is focused on the edge, then the distribution looks more like a peak and a tail rather than two peaks.

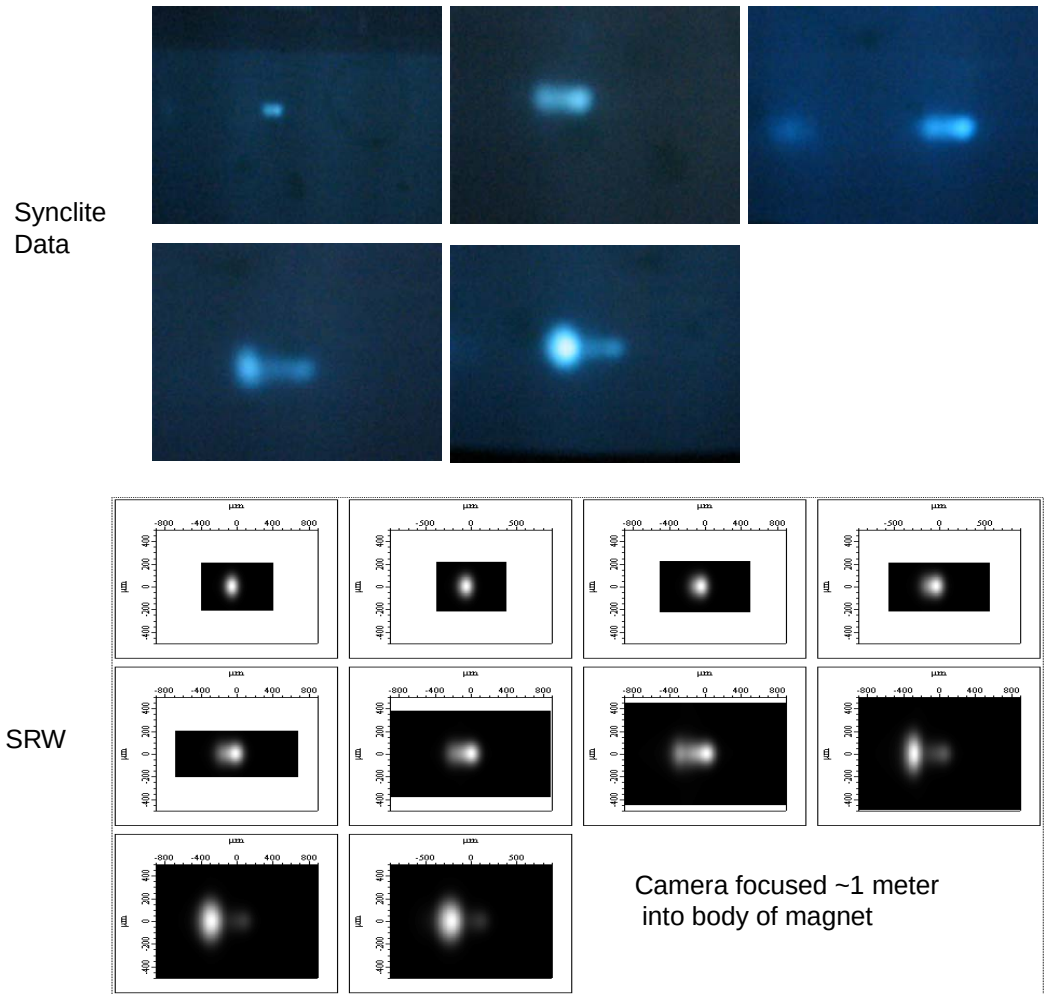

Figure 33: Progression of pbar pickoff mirror into the beampipe. The top is data and shows two peaks. The peak on the right is present when the mirror is out. As the mirror is inserted, the peak on the left grows and then dominates at the end. The peak on the left is the edge light. The SRW simulation on the bottom reproduces this behavior.

4.2.2 Wavelength Dependence and Diffraction Contribution

One significant contribution to the measured beam sigma comes from diffraction. The typical microscope diffraction formula, i.e. the radius of the airy disk, is

$$r_{airy} = 0.61\frac{\lambda}{NA} \qquad \textbf{(5)}$$

where *NA* is the numerical aperture of the objective lens (= $n \sin\theta$; n being refractive index of the medium before the lens), and λ is wavelength. For Synclite, *NA* is roughly the half angle of the light cone (since the optical elements are all much bigger than the light cone) which is 0.001 for the vertical plane and 0.0005 for the horizontal plane[6]. If one takes a more Gaussian approach, and says that the diffraction sigma is ½ the airy radius, then for Synclite at 400 nm,

[6] The half angle of the vertical light cone is approximately 1/γ, or ~1/1000, and the horizontal light cone is half the size of the vertical.

$$\sigma = 0.3\frac{\lambda}{NA}$$

$$\sigma_{vertical} = 120\ \mu m$$

$$\sigma_{horizontal} = 240\ \mu m \qquad \textbf{(6)}$$

A filter wheel was installed in the proton Synclite box with 4 narrowband wavelength filters [19]. Measurements of the vertical beam sigmas were taken with each of the filters at various camera positions and are plotted in Figure 34. In the main plot, the data have been slid along the x-axis by an amount

$$\Delta^{\{360,530,620\}} = S_i^{\{360,530,620\}} - S_i^{440} \qquad \textbf{(7)}$$

where S_i^X is the image distance at a wavelength of X nm. Thus each wavelength's data should have its minimum at the same value of x. This is another check of the behavior of the system. The numerical values for the theoretical shift in camera position are $\Delta^{\{360,530,620\}}$ = {-2.8 cm, 2.6 cm, 4.4 cm}.

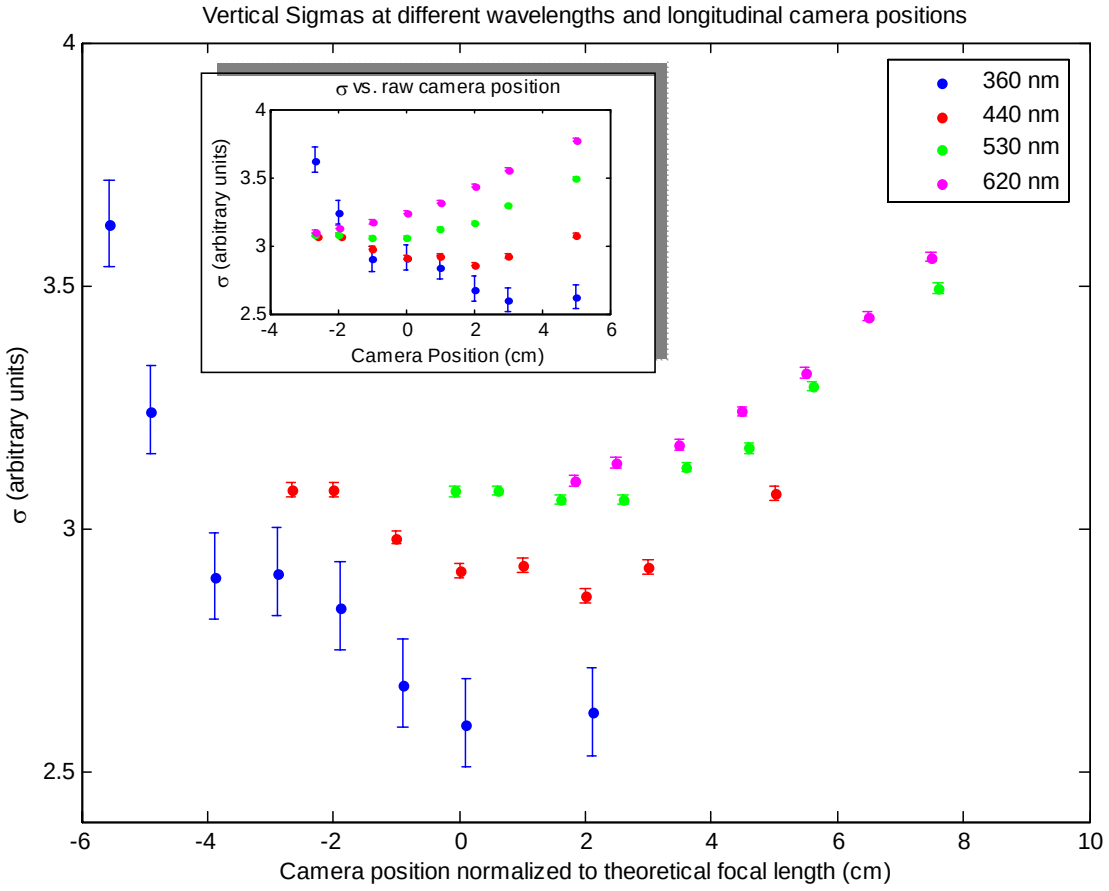

Figure 34: Vertical sigmas at 4 different wavelengths. The x coordinates of the inset plot is raw camera position. The x coordinates of the main plot have been adjusted for each wavelength to account for the theoretical change in the image distance with wavelength. So the minima should all lie at the same value of x on the main plot. (See the text for another description of this manipulation).

Figure 35 shows the variation of the sigma minima with wavelength after correcting the values of sigma for intensity effects and the changing optical gain. The plot compares data with simulation and also shows the functional behavior of the microscope formula.

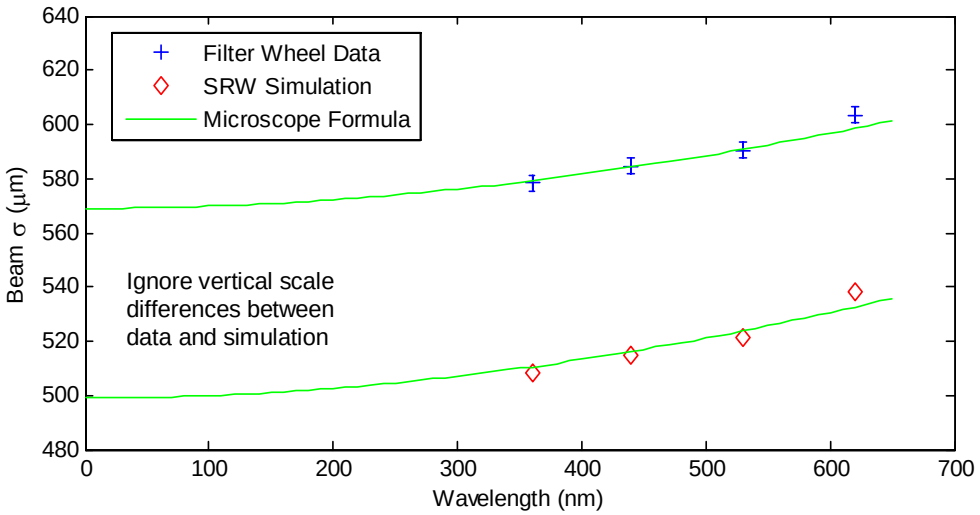

Figure 35: Plot comparing vertical sigmas from data with simulation and with the microscope formula. The data agree with the simulation and both agree with the microscope formula. The last point at 620 nm is a bit high and is probably due to the fact that the camera could not be moved far enough to reach the minimum.

Another method for determining the diffraction contribution is to use the SRW simulation to extract the expected width from diffraction. If one does this, one obtains Table 3 listing several methods and the results. The values obtained in this fashion agree with the microscope formula. The horizontal diffraction contribution is around 230 μm, and the vertical diffraction is around 130 μm.

Entity	Protons	Antiprotons Half Dipole Edge	Antiprotons Full Dipole Edge
SRW Parameters			
Object Distance (m)	7.777	5.022	5.422
Focal Length (m)	1.4746	0.7329	0.7329
Image Distance (m)	1.820	0.858	0.847
Optical Gain	4.274	5.852	6.398
Horizontal Beam Sigma (μm)	520	353	353
Vertical Beam Sigma (μm)	585	515	515
SRW Measurement of sigma and diffraction from sqrt(sigma^2 - beam^2)			
Horizontal Sigma (image plane) (μm)	132	69.3	65.9
Vertical Sigma (image plane) (μm)	141	90.5	83
Horizontal Sigma (object plane) (μm)	564	406	422
Vertical Sigma (object plane) (μm)	603	530	531
Horizontal Diffraction; quadrature difference (μm)	*219*	*200*	*231*
Vertical Diffraction; quadrature difference (μm)	*145*	*124*	*130*
SRW Measurement of diffraction directly (RMS of zero width beam image)			
Horizontal Diffraction (image plane) (μm)	48.7	40	40
Vertical Diffraction (image plane) (μm)	31.3	23	20
Horizontal Diffraction (object plane) (μm)	*208*	*234*	*256*
Vertical Diffraction (object plane) (μm)	*134*	*135*	*128*

Table 3: Listing of numerous parameters used in SRW to obtain the diffraction contribution. The diffraction was obtained in two ways: measure the sigma of a slice through the peak of the image and subtract out the known beam sigma (subtraction was done in a quadrature fashion), and measure the RMS of a slice through the peak of the diffracted image of a zero width beam. Both methods agree reasonably well.

The values of sigma in Table 3 are obtained by fitting vertical and horizontal slices through the peak. This differs from the Synclite system which fits profiles (the images are summed in each direction). Figure 36 shows the results of fitting profiles of simulated data at a variety of beam sizes. The proton data still agrees with the basic diffraction formula, but the antiproton data disagrees. If one looks in detail at the images, the discrepancy is understood as a variation in sigma with image position, due probably to the two magnet edges and more body light.

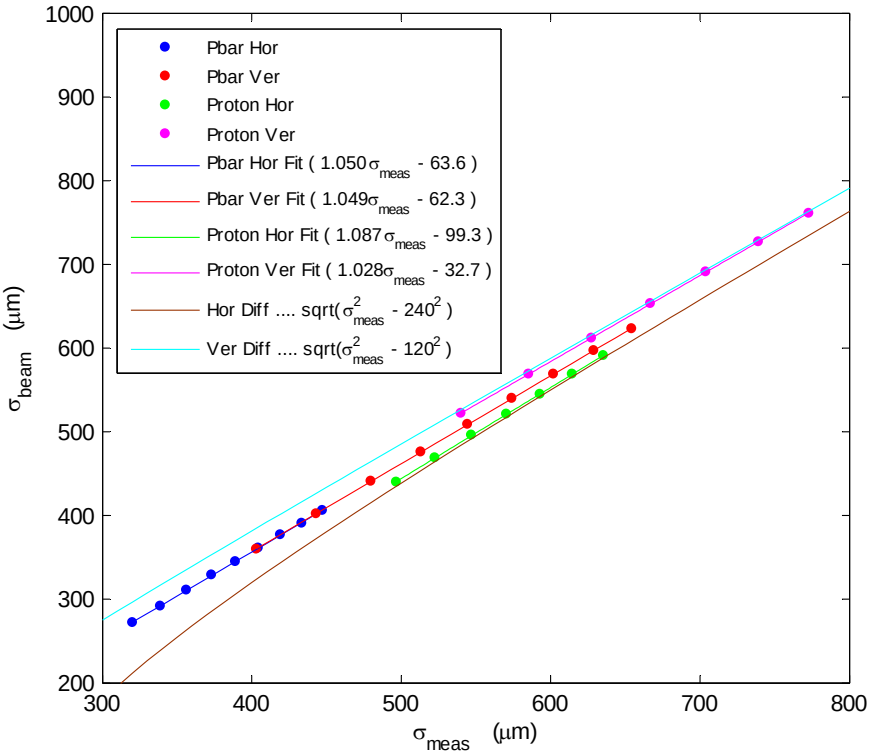

Figure 36: SRW simulation of beam sigma vs. measured sigma in both horizontal and vertical planes. The Hor Diff and Ver Diff curves are the expected shapes from point source diffraction alone. The other curves are linear fits to the data. The fact that the pbar points do not lie on the diffraction curves is probably due to some combination of more body light and two magnet edges contributing to the image, since those are the only differences between the proton and antiproton data.

4.2.3 Camera Focus

To obtain accurate images of the beam, the camera must be correctly focused. Naively, one would expect that the focal point is the location where the image is the narrowest. However, this only works for non-extended sources. In Synclite, the source is spread out longitudinally and the naive assumption no longer holds. Figure 37 shows the measured beam sigmas for various camera positions (image distances). The lines are the SRW simulated versions. Overlaid on the plots are arrows indicating where the theoretical focal points are located (taken from the simulation). The discrepancies between data and simulation may be due to differences in the fits between the front end and SRW.

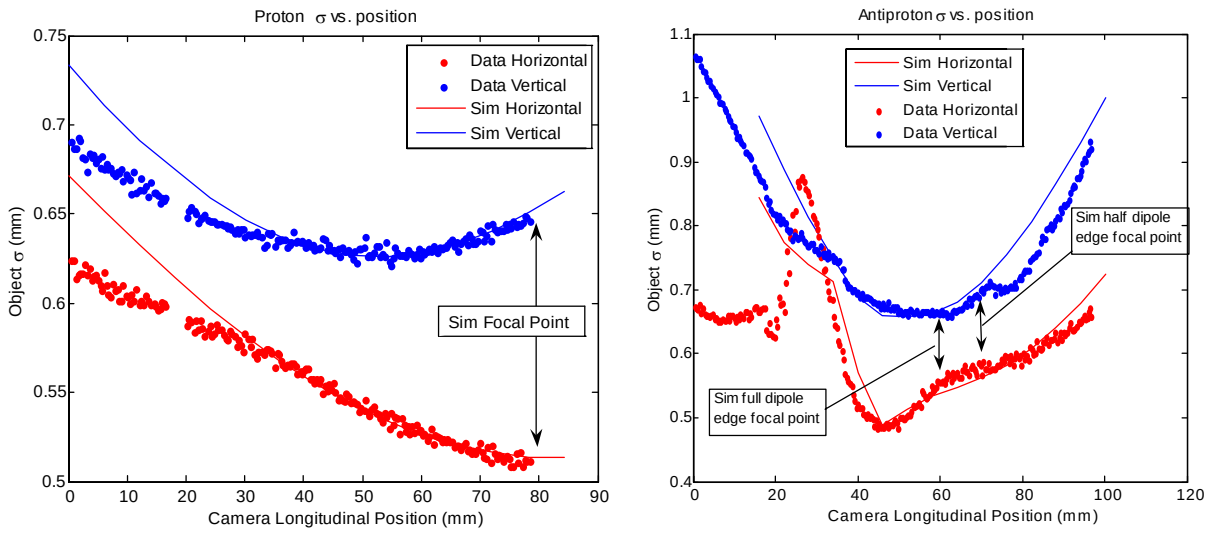

Figure 37: Measured beam sigma for protons and antiprotons as a function of longitudinal camera position. The lines are the simulated sigmas. There are some discrepancies which may be due to different fitting techniques, but the overall shapes are pretty good. The theoretical focal points are shown by the arrows. The antiprotons have 2 magnet edges and thus have 2 focal points. The most striking feature is that the focal points do not lie at the minimum.

4.3 Global Scale

To determine the global scale, one must know the optical gain of the system (which was discussed above), and the pixel size of the camera, or in the case of Synclite, the framegrabber. The camera in Synclite produces an analog RS-170 video signal from its visible pixels. The current cameras have a visible area of 753 horizontal by 480 vertical. The RS-170 standard specifies 485 visible horizontal lines (vertical pixels), a 4:3 aspect ratio (implying ~647 horizontal pixels), and 52.66 μs for the duration of the visible part of the horizontal line. The camera outputs all 753 pixels into that horizontal line, but the framegrabber hardware at the other end digitizes it assuming a standard 647 pixels. This only affects the horizontal pixel size, since the vertical pixel size is defined by the sync pulses in the video signal and is not adjustable. Thus the horizontal size of a pixel at the DAQ end is

$$pixel_{framegrabber} = pixel_{camera} \times \frac{753}{647} \qquad \textbf{(8)}$$

For the Synclite system, the camera pixels are 11.5 μm square leading to a framegrabber pixel size of 13.4 μm (h) × 11.5 μm (v).

The global distance scale can in principle be checked by comparison with Beam Position Monitor (BPM) data. The new BPMs have a precision of tens of microns, and the BPM scale was confirmed to be very close to 1 by the fits for the Tevatron lattice functions. Thus we have

$$\begin{aligned} \mu_{SL} &= k\mu_B + \Delta_{SL} \\ \mu_{BPM} &= \mu_B + \Delta_{BPM} \\ \mu_{SL} &= k\mu_{BPM} + (\Delta_{SL} - k\Delta_{BPM}) \end{aligned} \qquad \textbf{(9)}$$

where μ is the position, Δ is an offset and k is the fractional scale error of Synclite. Hence the Synclite scale factor k is just the slope of a linear fit to the Synclite vs. BPM data. In practice there are drifts and apparent discrete jumps even within a store that makes it difficult to fit a

single line. In addition, the antiproton BPM measurements are unreliable. An alternative is to use orbit bumps to move the beam and compare with BPM data. This may be done in the future.

5 Results

The results come in the form of a comparison with the flying wires. For completeness, the emittance is calculated as follows

$$\varepsilon = \frac{6\gamma}{\beta}\left(\sigma^2 - D^2\left\langle\left(\frac{dp}{p}\right)^2\right\rangle\right) \pi \text{ mm mr} \qquad \textbf{(10)}$$

For the vertical emittance, the dispersion term *D* is taken to be zero. The dp/p term is obtained from the SBD device, T:SBDxMS, where x is P for protons and A for antiprotons.

5.1 Present System

Figures 38 and 39 show the results of emittance determinations from Synclite. The former plot shows the fitted sigmas of the images in raw pixels. The latter plot is a comparison of Synclite emittance with that determined by the Flying Wire system. There is a 30-40% discrepancy in the Pbar horizontal measurement.

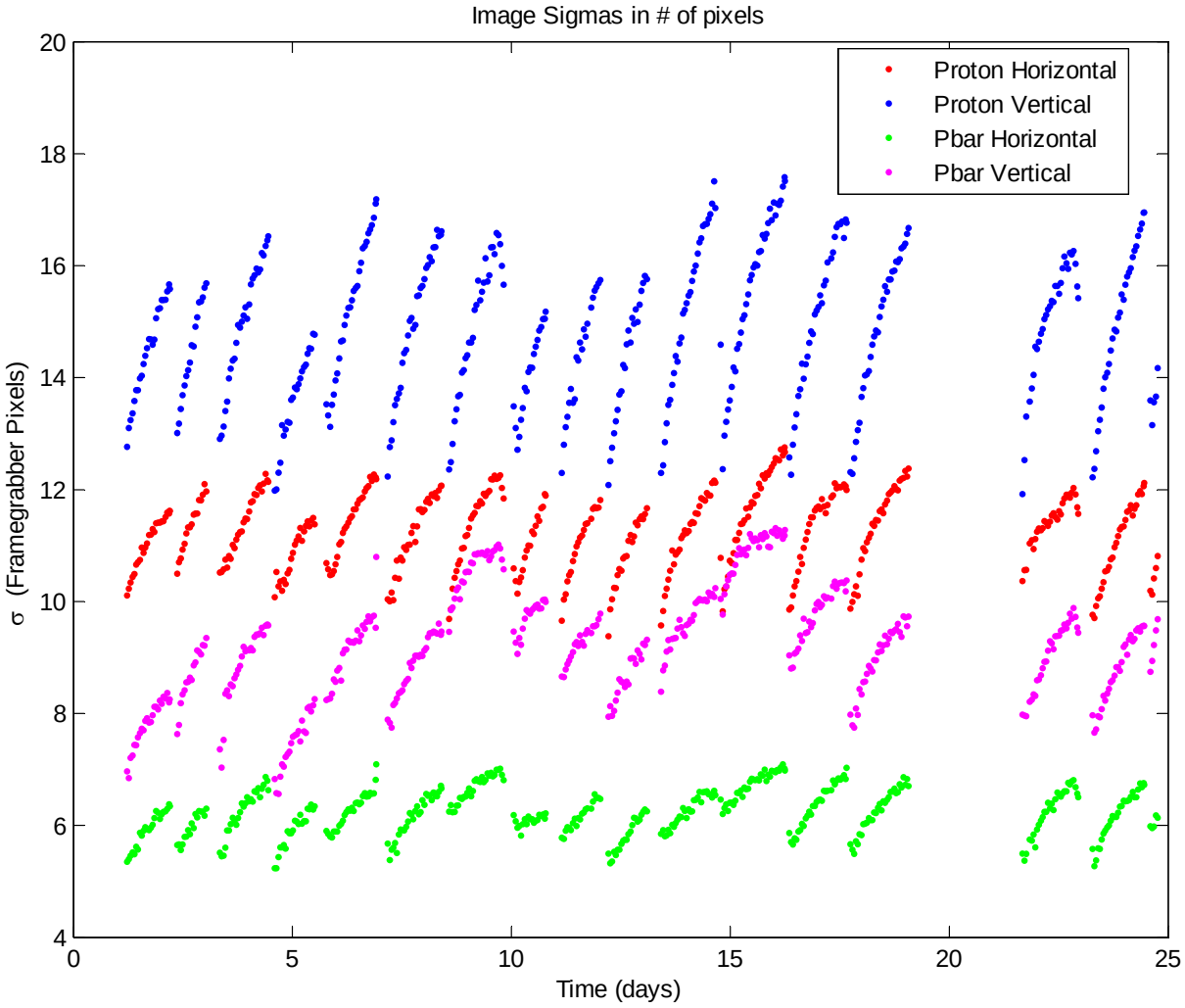

Figure 38: Image sigmas in units of framegrabber pixels. Remember that sigma is defined such that 95% of the Gaussian is contained in a width of 4 sigma. Thus at least 20 points are effectively used in determining the Gaussian fit parameters for even the smallest images (pbar horizontal). This should alleviate any concern that there are distortions due to the small number of pixels used in the fit.

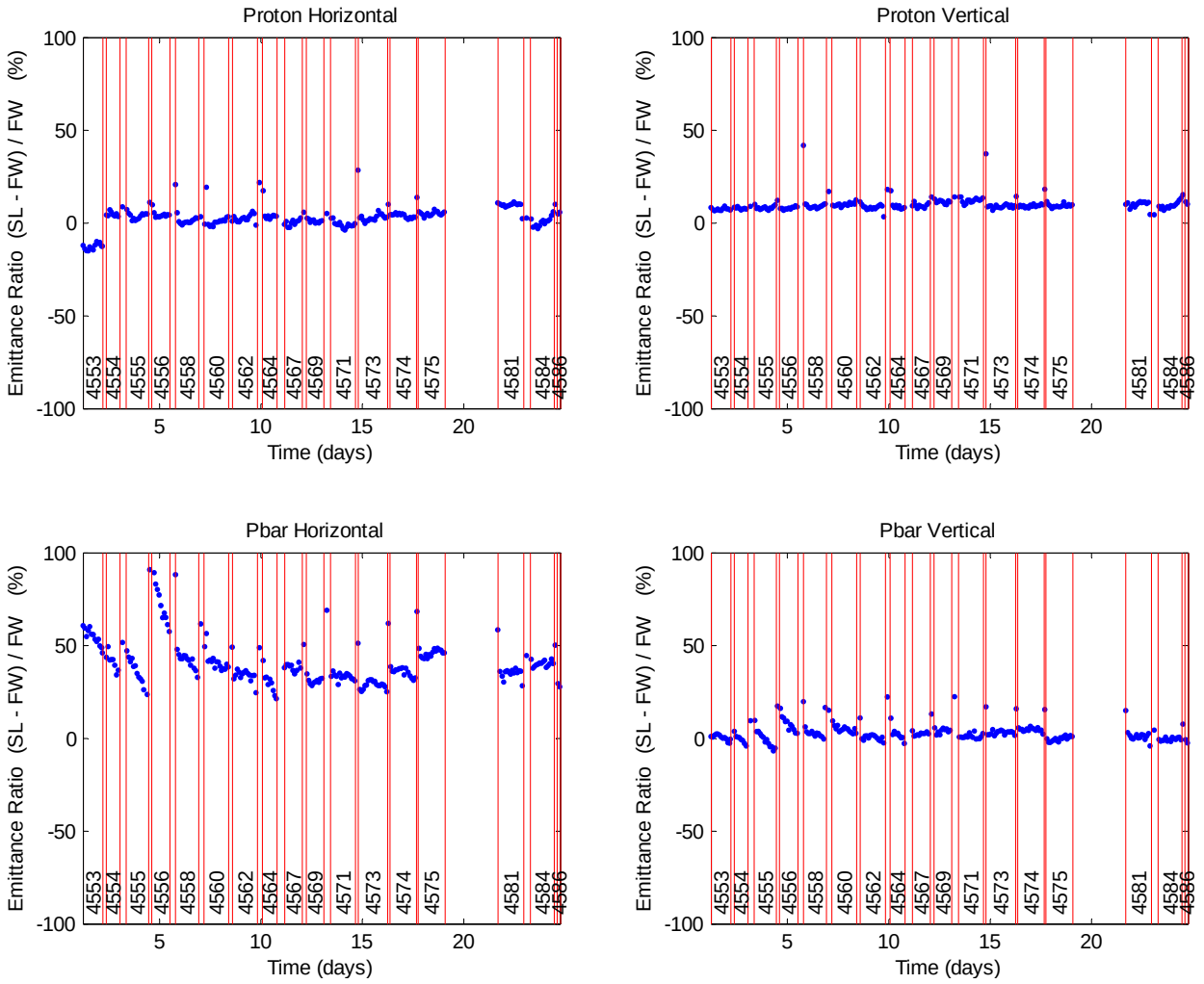

Figure 39: Comparison of Synclite emittance measurements with flying wire measurements. The Pbar Horizontal emittance has ~30-40% discrepancy. The red vertical lines delineate store boundaries and the rotated numbers are the store numbers.

Figure 40 is a comparison of the Synclite and Flying Wire horizontal pbar sigmas for each bunch from Store 4556. The tail bunch in each train had much larger emittance growth. The odd thing is that the relative difference between bunches does not agree in the two systems.

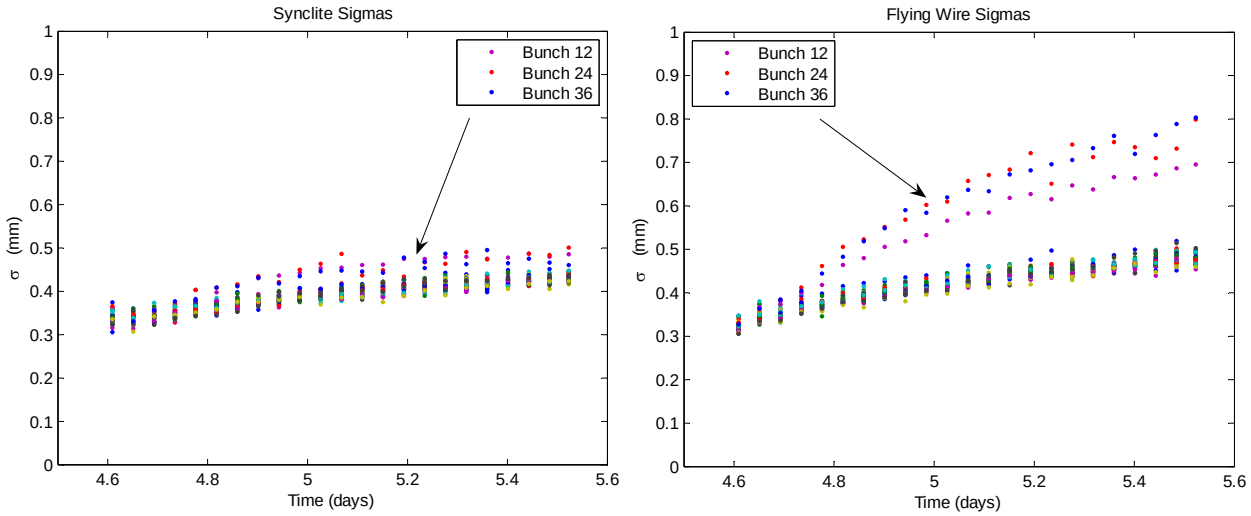

Figure 40: Bunch by bunch difference between Synclite and Flying Wire horizontal pbar sigmas. The ratio of the beta functions (sqrt(β_{SL} / β_{FW}) ~ 0.68) is such that the Synclite sigmas should be about 32% smaller than the Flying Wires. The tail bunches have much larger emittance growth as seen in this plot, but the growth relative to the other bunches is not equivalent in the two systems.

5.2 Post 2006 Shutdown

Figures 41 and 42 show comparisons of Flying Wire and Synclite emittances just after the 2006 shutdown. The Synclite pbar horizontal sigmas seem to have decreased since before the shutdown.

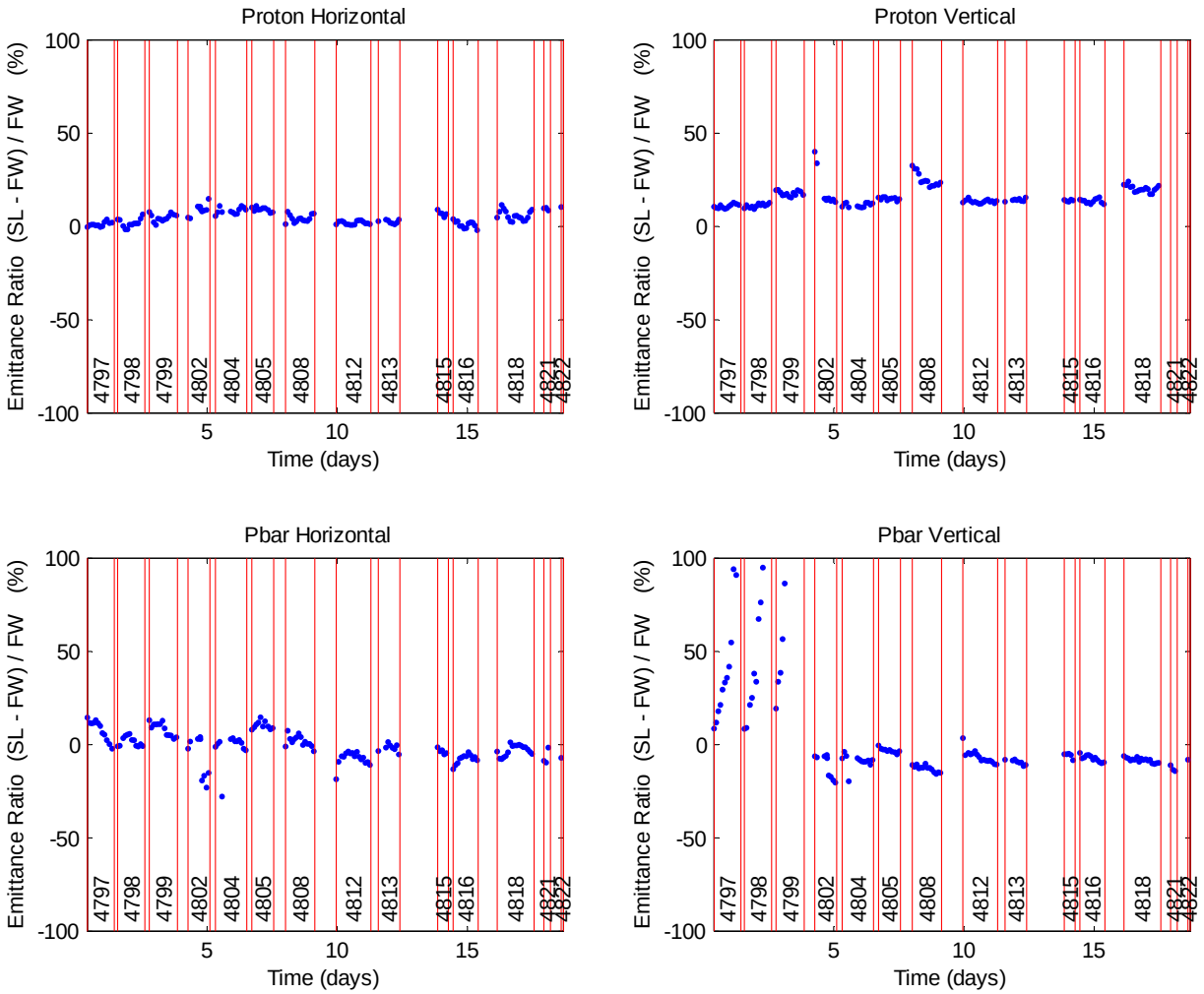

Figure 41: Comparison of Flying Wire and Synclite emittances for the first stores after the 2006 shutdown. The pbar horizontal emittances are in much better agreement after the shutdown.

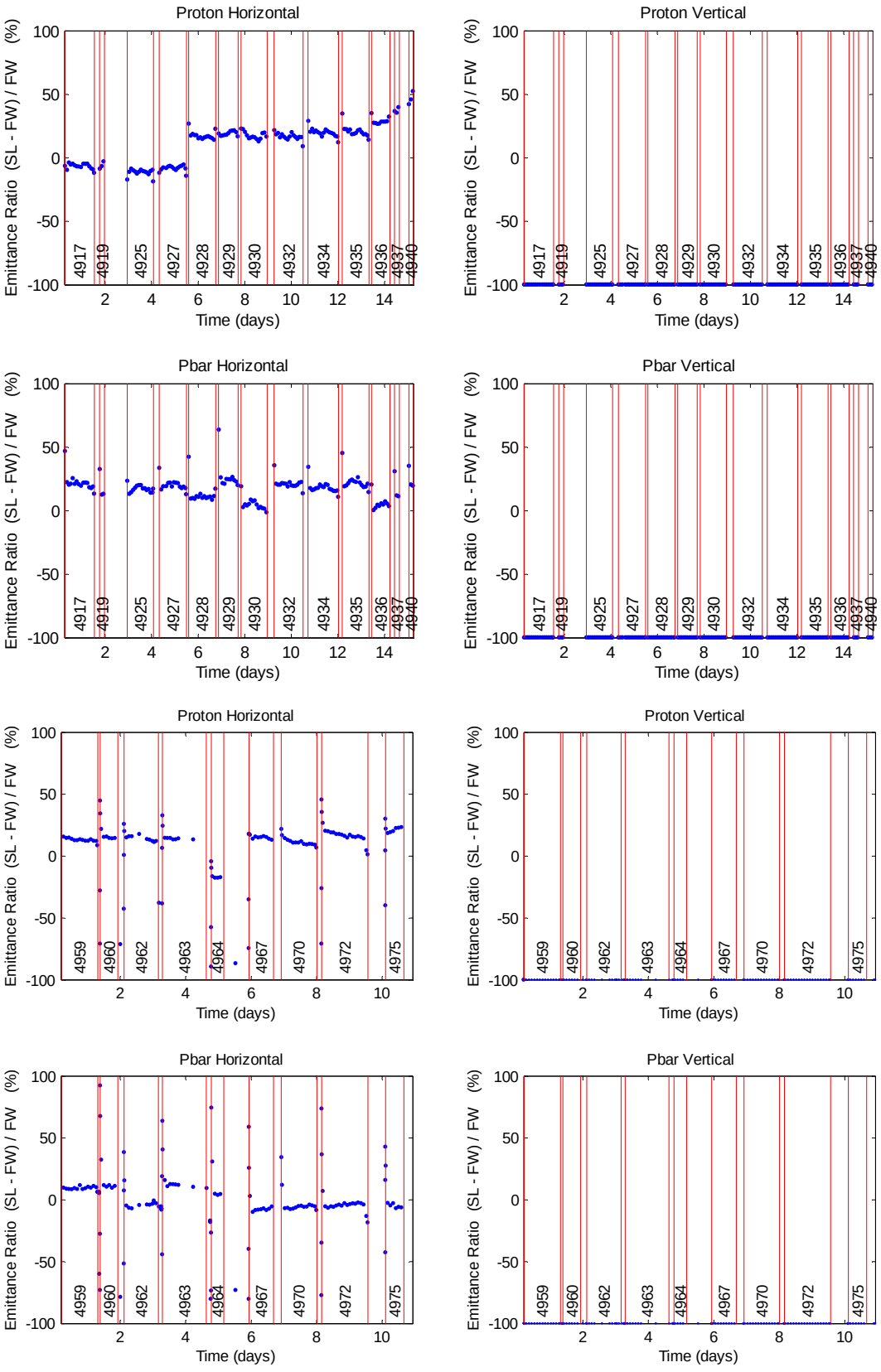

Figure 42: Two more samples of Synclite / Flying Wire comparisons. In both these samples, the Flying Wire vertical wire was incapacitated. One thing to notice is the variation in these plots from store to store which is in the neighborhood of 20% in some cases. This is presumably due to variations in the lattice since the instruments are not changing.

6 Acknowledgements

Thanks to Stephen Pordes for pushing to understand the Synclite system. Thanks to Alan Hahn and Harry Cheung for useful pieces of information about the system and for installing and maintaining the original Synclite. Thanks to Carl Lundberg and Dale Miller for all manner of technical support. And especially thanks to Eugene Lorman for overhauling and modernizing the Synclite DAQ system and for rapidly responding to all my various requests for changes and enhancements to LabVIEW.

7 References

[1] A. Hahn, P. Hurh, “Results From An Imaging Beam Monitor In The Tevatron Using Synchrotron Light”, **BEAMS-DOC-185**.

[2] A. Hahn, P. Hurh, “Results From A Prototype Beam Monitor In The Tevatron Using Synchrotron Light”, **BEAMS-DOC-186**.

[3] A. Hahn, **BEAMS-DOC-418**, Curves of spectral energy density of synchrotron radiation. The calculations are based on formulas by R. Coisson [10], which make certain assumptions which are not entirely valid at a beam energy of 980 GeV, or even 900 GeV for that matter. As such they are a factor of 5-10 too small.

[4] H. W. K. Cheung, A. Hahn, A. Xiao, “Performance Of A Beam Monitor In The Fermilab Tevatron Using Synchrotron Light”, **BEAMS-DOC-587**.

[5] H. W. K. Cheung and S. Pordes, “Studies of the Synclite Scale”, **BEAMS-DOC-466**.

[6] A. Jansson, S. Pordes, **BEAMS-DOC-417**, Diagram showing Synclite dimensions. The dimensions in this reference are superseded by the dimensions in this document (see Section 4.2).

[7] A. Hahn, H. W. K. Cheung, **BEAMS-DOC-415**, pictures from the Synclite boxes.

[8] H. W. K. Cheung, “Second Beam Orbit Study To Calibrate The Synclite Scale”, **BEAMS-DOC-459**.

[9] H. W. K. Cheung, E. Lorman, D. Miller, S. Pordes, K. Schultz, “Synclite Study During The December Shutdown”, **BEAMS-DOC-987**. TeV Group Talk, but with lots of pictures, in particular, of the inside of the Synclite beampipe.

[10] R. Coisson, “Angular-spectral distribution and polarization of synchrotron radiation from a ‘short’ magnet”, Phys. Rev. A **20** (1979) 524.

[11] J.D. Jackson, Classical Electrodynamics, John Wiley and Sons, (1962), Ch. 14.

[12] J. Bosser *et al.*, “Proton beam profile measurements with synchrotron light”, Nucl. Inst. and Meth. **164** (1979) 375.

[13] *Synchrotron Radiation Workshop (SRW)*
http://www.esrf.fr/Accelerators/Groups/InsertionDevices/Radiations/Software/SRW
SRW handles calculation of the synchrotron radiation wavefront, and propagation through optical elements. It runs from within an application called Igor Pro (see next reference).
O. Chubar, P. Elleaume, "Accurate And Efficient Computation Of Synchrotron Radiation In The Near Field Region", proc. of the EPAC98 Conference, 22-26 June 1998, p.1177-1179.

[14] *Igor Pro* -- WaveMetrics, Inc. A data analysis program similar to MATLAB, or MATHCAD. http://www.wavemetrics.com/

[15] For a description of the Synclite DAQ, see **BEAMS-DOC-1262**, and **BEAMS-DOC-1738**. Detailed cable connections for the Synclite and AGI systems can be found in **BEAMS-DOC-1098**. A JAVA-based viewer is described in **BEAMS-DOC-1973.**

[16] Aluminized Mirror. Loss is typically 10%.

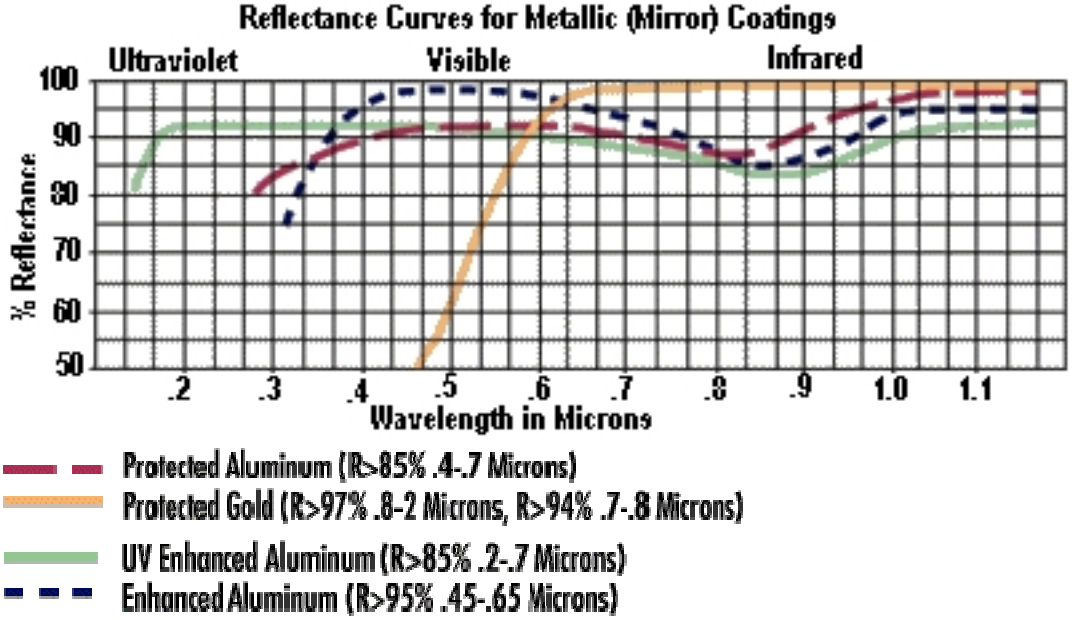

[17] MDC Vacuum Products quartz window #450023 for antiproton and #450024 for proton. The transmission of the quartz window is curve number 2 below (90% for 400-500nm).

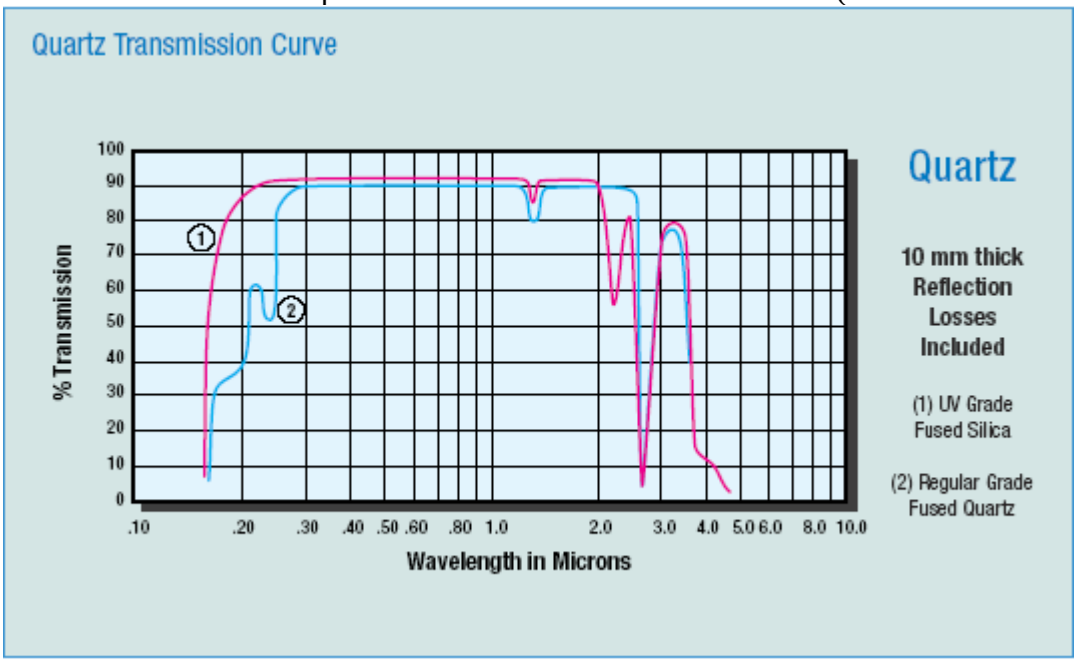

[18] Proton system lens is Oriel (now Spectra-Physics) 2” DIA plano convex lens #40825 made of BK7 glass with 1500 mm focal length and 1495.6 mm back focal length. Antiproton system lens is Oriel (now Spectra-Physics) 2” DIA plano convex lens #40815 made of BK7 glass with 750 mm focal length and 745.7 mm back focal length. All focal lengths are measured at 589 nm. Transmittance for BK7 glass is shown below (93% for 400-500nm).

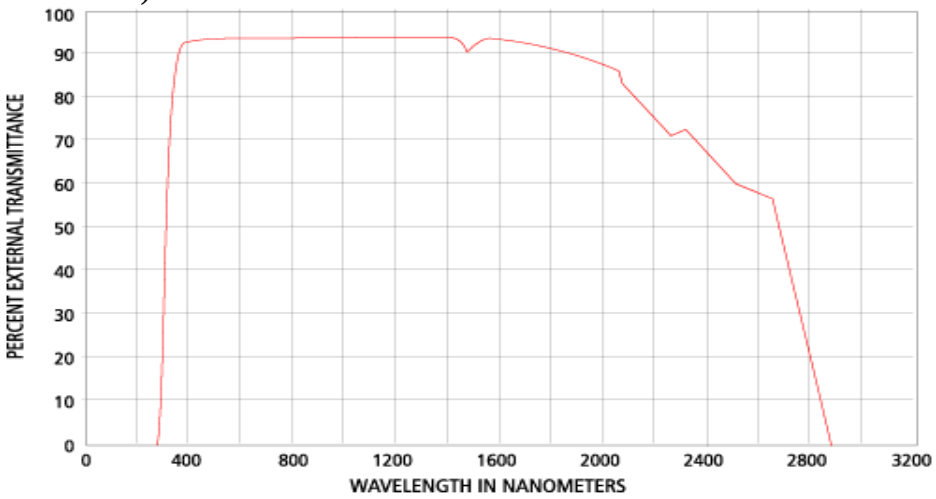

[19] Thorlabs non-polarizing beam splitter #BS013 constructed of two BK7 glass prisms with antireflection coatings on the entrance and exit surfaces. The left plot below shows the transmittance, *T*, of forward beam for the two polarization states through the beamsplitting coating between the prisms. The right plot shows the reflectance, *R*, for a typical broadband antireflection coating. So the total transmittance for the forward light path would be *(1-R)*T*(1-R)*.

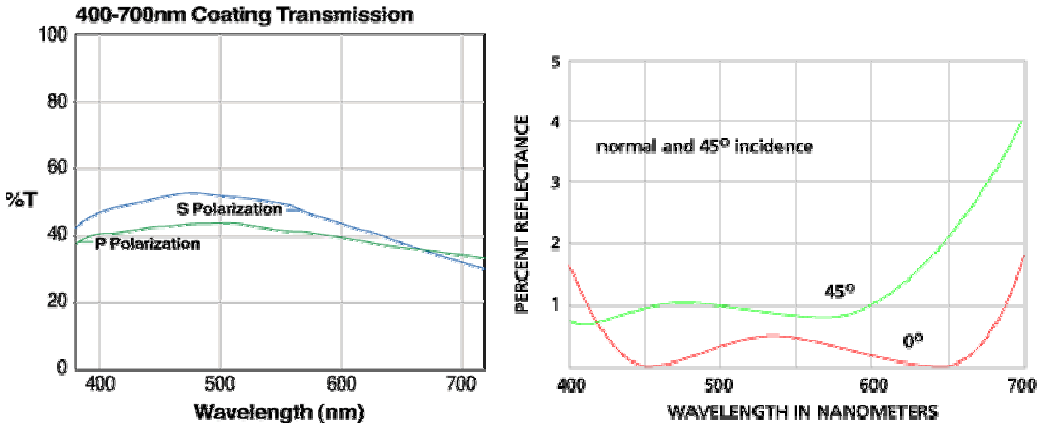

[20] R. Thurman-Keup, “Abort Gap Monitoring Utilizing Synchrotron Light”, **BEAMS-DOC-1390.**

[21] Hamamatsu gated image intensifier V6887U-02. This plot shows the photocathode efficiency of the intensifier.

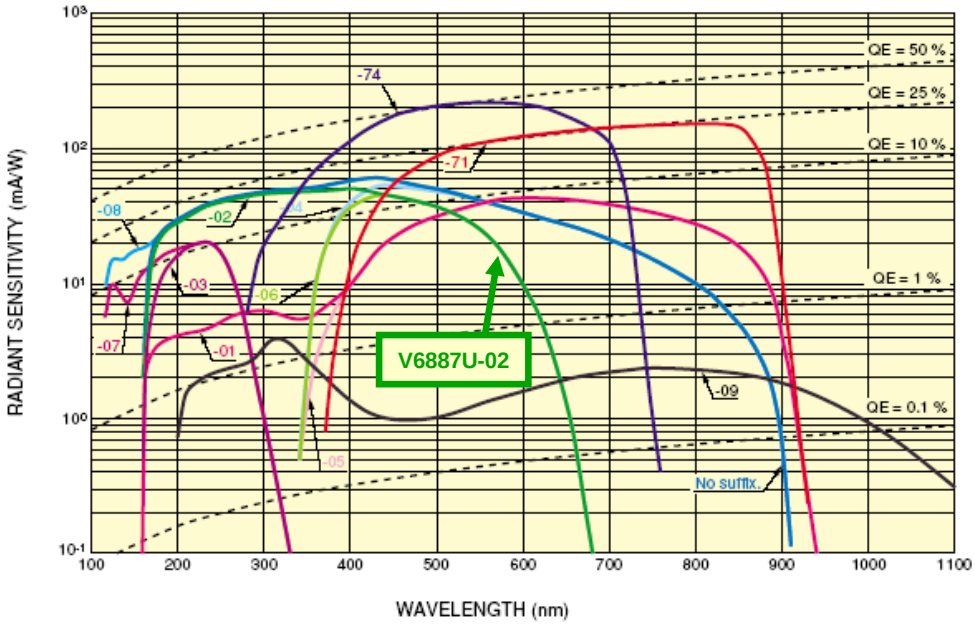

[22] Thermo-electron (formerly Spectra-Physics) CID camera: model # CID3710DX12. This is a monochrome CID type solid state camera with 11.5 µm × 11.5 µm pixels.

[23] Wavelength filters for proton and pbar systems. The proton box has a filter wheel containing 4 Thorlabs filters: 360nm (Part # FB360-10), 440nm (FB440-10), 530nm (FB530-10), 620nm (FB620-10), each of which has a 10nm bandwidth. The pbar box has a single Melles-Griot 440nm filter (Part # 03 FIV 026) which has a bandwidth of 40nm. The following plots show the wavelength transmission for each of these filters.

Antiproton Filter

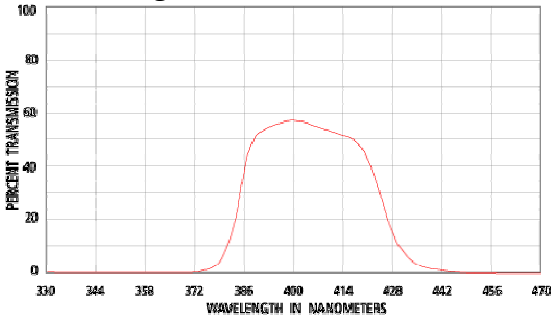

Proton Filter Wheel Filters

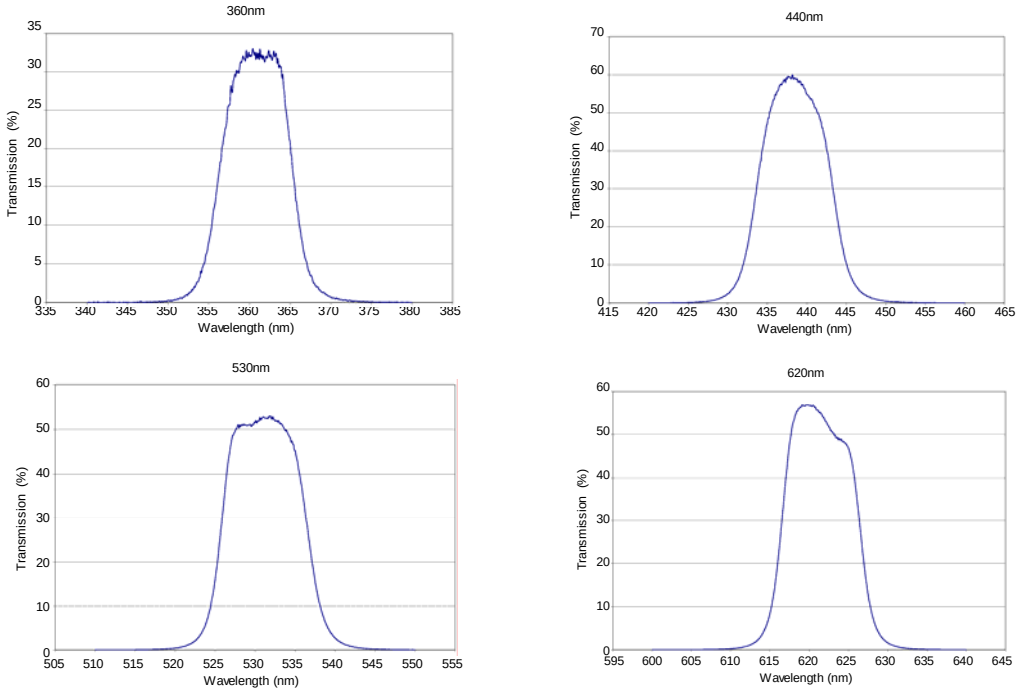

[24] The intensifier/CID camera is mounted on a Parker-Daedal (Parker Industries, Daedal Division) Linear Motion Table, part # 506061S-LH. The screw has 5 threads / inch.